J. Fluid Mech. (2001), *vol.* 434, *pp.* 243–271. Printed in the United Kingdom

© 2001 Cambridge University Press

Instability of a gravity-modulated fluid layer with surface tension variation

By J. RAYMOND LEE SKARDA†

NASA Glenn Research Center Cleveland, OH 44135, USA

(Received 28 June 2000 and in revised form 3 October 2000)

Gravity modulation of an unbounded fluid layer with surface tension variations along its free surface is investigated. The stability of such systems is often characterized in terms of the wavenumber, α and the Marangoni number, Ma. In (α, Ma) parameter space, modulation has a destabilizing effect on the unmodulated neutral stability curve for large Prandtl number, Pr, and small modulation frequency, Ω, while a stabilizing effect is observed for small Pr and large Ω. As $\Omega \to \infty$ the modulated neutral stability curves approach the unmodulated neutral stability curve. At certain values of Pr and Ω, multiple minima are observed and the neutral stability curves become highly distorted. Closed regions of subharmonic instability are also observed. In $(1/\Omega, g_1 Ra)$-space, where g_1 is the relative modulation amplitude, and Ra is the Rayleigh number, alternating regions of synchronous and subharmonic instability separated by thin stable regions are observed. However, fundamental differences between the stability boundaries occur when comparing the modulated Marangoni–Bénard and Rayleigh–Bénard problems. Modulation amplitudes at which instability tongues occur are strongly influenced by Pr, while the fundamental instability region is weakly affected by Pr. For large modulation frequency and small amplitude, empirical relations are derived to determine modulation effects. A one-term Galerkin approximation was also used to reduce the modulated Marangoni–Bénard problem to a Mathieu equation, allowing qualitative stability behaviour to be deduced from existing tables or charts, such as Strutt diagrams. In addition, this reduces the parameter dependence of the problem from seven transport parameters to three Mathieu parameters, analogous to parameter reductions of previous modulated Rayleigh–Bénard studies. Simple stability criteria, valid for small parameter values (amplitude and damping coefficients), were obtained from the one-term equations using classical method of averaging results.

1. Introduction

Under certain conditions, such as thin liquid films or in a low-gravity environment, surface tension variations along a free surface may induce convection, referred to as thermocapillary convection. Thermocapillary phenomena are important to terrestrial applications such as coatings and drying processes as well as potential microgravity technologies such as crystal growing and materials processing applications. Onset of thermocapillary convection in the form of an extended Marangoni–Bénard problem remains an active topic of study, in part due to its relative simplicity in terms of a motionless basic state and constant (or time-periodic) coefficients. The popularity of such models also comes from the understanding and physical insight they have

† Present address: ICASE, NASA Langley Research Center, Hampton VA 23681-2199, USA.

https://doi.org/10.1017/S0022112001003603 Published online by Cambridge University Press

provided for a broad range of physical phenomena (Pimputkar & Ostrach 1981; Ostrach 1982; Davis 1987; Legros *et al.* 1990; Koschmieder 1993). Bénard-type models have also been used to examine modulation effects such as temperature or gravity modulation; however Marangoni–Bénard problems have received far less attention than Rayleigh–Bénard problems.

Gershuni & Zhukhovitskii (1963) and Venezian (1969) considered the effect of temperature modulation of the Rayleigh–Bénard problems where buoyancy drives convection. Two papers, Gershuni, Zhukhovitskii & Iurkov (1970) and Gresho & Sani (1970) address gravity modulation of the Rayleigh–Bénard problem. Gershuni, Zhukhovitskii & Iurkov (1970) considered the linear stability of an unbounded fluid layer and fluid within a vertical circular cylinder with modulation of both the mean vertical temperature gradient and the vertical component of gravity, while Gresho & Sani (1970) studied both linear and nonlinear behaviour of the gravity-modulated unbounded layer. In both studies, a one-term Galerkin expansion reduced the equations to a single second-order ordinary differential equation. Applying a direct analogy to the viscously damped pendulum with an oscillating vertical support, Gresho & Sani (1970) recast the problem in terms of the Mathieu equation, reducing the number of parameters affecting the system behaviour from six (fluid transport) to three (Mathieu). These earlier studies were often associated with other fundamental problems such as Taylor instability, pendulum analogies, and fluid control techniques.

Renewed interest in modulated Bénard-type problems over the past decade has been motivated by study of fluid and materials processing systems in low-gravity environments, and the potential impact of residual accelerations and vibrational mechanisms on these systems. An enormous amount of transient acceleration measurements has been recorded from flights or missions on board various Earth orbiting platforms. Results from these data have been summarized to characterize the residual acceleration environments, while actual flight data are accessible for further analysis or transient simulation activities (cf. DeLombard 1999; McPherson & Hrovat 2000). The gravity level on board orbital laboratories is not constant, and the response of fluid or materials processing systems continues to be an active topic of research (Monti, Langbein & Favier 1987; Alexander 1990; Nelson 1994). In general, the time-dependent part of the residual acceleration, *g-jitter*, varies randomly in magnitude and direction. With the exception of attitude adjustments, these disturbances are usually transmitted as structural vibrations, eventually to the support structure or container walls of the fluid system in question, such as fuel tanks, or laboratory experiments. Therefore, the actual excitation experienced by the fluid may sometimes be approximated by a harmonic forcing with the frequency of the resonant structural mode.† More precisely, for small disturbances (e.g. displacements), broad-band random excitation near a highly resonant mode gives a narrow-band response centred on the natural frequency (Newland 1993). Clearly, the random nature, combination tones (and other nonlinear effects), and orientation cannot be ignored. However, a Floquet analysis of the approximated system, linearized with periodic excitation, is a good first step. In addition to their theoretical merits, these analyses often provide practical insight for appropriate physical conditions.

Several recent studies concerned with g-jitter in space-related applications, have applied Floquet theory to characterize stability behaviour in the context of a modulated Bénard-type problem. Murray, Coriell & McFadden (1991) and Wheeler *et al.*

† In the case of broader band fluctuations, multiple resonant modes can certainly occur.

https://doi.org/10.1017/S0022112001003603 Published online by Cambridge University Press

(1991) treated the gravity-modulated onset of convection problem with respect to directional solidification. Certain combinations of modulation amplitudes and frequencies were found to stabilize the unmodulated fluid layer that would normally be unstable, or conversely destabilized a fluid layer whose unmodulated state is stable. Gravity-modulated double-diffusive convection was examined by Saunders *et al.* (1992). Terrones & Chen (1993) performed a comprehensive analysis of the effects of gravity modulation in both double-diffusive, and binary fluid systems where Soret effects occur. More recently, Gershuni *et al.* (1997) have applied the method of averaging to study modulation in binary fluid systems in the presence of high modulation frequencies. For all modulated studies cited thus far, buoyancy is the stratifying agency which incites instabilities.

Recently, the effects of modulation have been examined in systems where flow is driven by surface tension variation along a free surface (Or & Kelly 1995; Kelly & Or 1998; Or 1997). Although not specifically concerned with gravity modulation, these papers appear to be among the first to consider modulation effects in such systems. They have investigated the effect of shear and temperature modulation on the Marangoni–Bénard problem and noted interesting behaviour associated with surface deformation. For example, shear modulation due to an oscillating lower (rigid) boundary, destabilized the long-wavelength mode but stabilized the finite-wavelength modes. They found shear modulation could stabilize both finite- and long-wavelength modes while thermal modulation is effective in stabilizing the finite mode (Kelly & Or 1998). A preliminary thermocapillary study of gravity modulation for single- and double-diffusive systems with flat non-deformable free surface has also been reported by Skarda (1998*a*).

In this paper, parametric excitation of an unbounded fluid layer with surface tension variation along the free surface is considered. The work is subject to the same restrictions as those of studies cited above, and represents a similar step towards characterizing vibrational g-jitter effects in reduced-gravity environments. This paper focuses on the Marangoni–Bénard problem, and how a fluid layer responds to gravity modulation or time-periodic accelerations, which are imposed in the direction of the basic temperature gradient. The problem is formulated in § 2 where Floquet theory is applied to examine the stability of the modulated system using a spectral collocation approach to discretize the relevant systems of equations, and results are presented in § 3. A brief investigation of and comparison with the modulated Rayleigh–Bénard problem is also provided in § 3.3. In § 4 the mechanical analogy used by Gresho & Sani (1970) for the Rayleigh–Bénard problem is extended to the Marangoni–Bénard problem. Finally simple equations based on method of averaging in connection with the one-term Galerkin formulation, are developed in § 4.3 that predict the modulation behaviour of the fundamental instability boundary.

2. Formulation of equations and boundary conditions

An unbounded fluid layer with dimension $0 \leqslant x_3^* \leqslant d$ is considered. The governing equations, continuity, momentum and energy equations, for incompressible flow are

$$\frac{\partial U_i^*}{\partial x_i^*} = 0, \tag{2.1}$$

$$\frac{\partial U_i^*}{\partial t^*} + U_j^* \frac{\partial U_i^*}{\partial x_j^*} = \frac{-1}{\rho_o} \frac{\partial p^*}{\partial x_i^*} - \frac{\rho}{\rho_o} g_i^*(t^*) \delta_{i3} + \nu \frac{\partial^2 U_i^*}{\partial x_j^* \partial x_j^*}, \tag{2.2}$$

https://doi.org/10.1017/S0022112001003603 Published online by Cambridge University Press

$$\frac{\partial T^*}{\partial t^*} + U_j^* \frac{\partial T^*}{\partial x_j^*} = \mathfrak{D} \frac{\partial^2 T^*}{\partial x_j^* \partial x_j^*}, \tag{2.3}$$

where δ_{ij} is Kronecker's delta, $i = 1, 2, 3$ and * denotes dimensional quantities. The dependent variables U_i^* and T^* are the velocity and temperature respectively. The time-dependent body force term is periodic, of the form $g^*(t) = g_o^* + g_1^* \cos(\Omega^* t^*)$. Density, ρ, is computed using the Boussinesq approximation, $\rho = \rho_o\{1 - \beta(T^* - \bar{T}_0^*)\}$, where β is the thermal expansion coefficient. The reference temperature chosen for the buoyancy term is that of the lower surface, $\bar{T}_0^*$. The kinematic viscosity, ν, and thermal diffusivity, $\mathfrak{D}$, are assumed constant. Impenetrable and no-slip velocity conditions are applied, and a constant temperature is imposed at the lower surface, $x_3^* = 0$.

At $x_3^* = 0$ (bottom)

$$U_i^* = 0, \quad T^*(0) = \bar{T}_0^*, \quad (\text{for } i = 1, 2, 3), \tag{2.4a, b}$$

The upper surface, at $x_3^* = d$, is flat and non-deformable leading to

$$U_3^* = 0, \tag{2.5a}$$

while tangential stress balances are given by

$$\mu \left(\frac{\partial U_3^*}{\partial x_j^*} + \frac{\partial U_j^*}{\partial x_3^*} \right) = -\gamma \frac{\partial T^*}{\partial x_j^*}. \tag{2.5b, c}$$

The heat flux condition is given by

$$-\rho c_p \mathfrak{D} \frac{\partial T^*}{\partial x_3^*} = Q^*. \tag{2.5d}$$

In (2.5) $j = 1, 2$; and μ and c_p are the dynamic viscosity and specific heat, respectively, with constant values. Surface tension, σ, is approximated as a linearized function of T^*, $\sigma = \sigma_0 - \gamma(T^* - \bar{T}_1^*)$ where the surface tension variation with temperature, γ, is defined as $\gamma = -(\partial\sigma/\partial T^*)_{c^*, P^*}$ (Adamson 1982). Q^* is the heat flux to the environment at the free surface.

The velocity and temperature basic state profiles are $\bar{U}^* = 0$ and $\bar{T}^*(x_3^*) = \bar{T}^*(0) - \Delta\bar{T}^* x_3/d$ where the difference quantities of the form Δy^* are defined as $\Delta y^* = y^*(0) - y^*(d)$. Following Gresho & Sani (1970), Gershuni *et al.* (1970) and Joseph (1976), the equations are linearized and then non-dimensionalized. Reference values used to non-dimensionalize the resulting disturbance equations are d, $\mathfrak{D}/d$, $d^2/\mathfrak{D}$, and $\Delta\bar{T}^*$, for length, velocity, time, and temperature, respectively. By assuming solutions of the form

$$(u(x_i, t), \theta(x_i, t)) = (w(x_3, t), \phi(x_3, t)) \exp(\mathrm{i}(\alpha_1 x_1 + \alpha_2 x_2))$$

for the perturbation variables, velocity, u, and temperature, θ, the following disturbance equations of x_3-momentum and energy are obtained.

$$(\mathrm{D}^2 - \alpha^2)\dot{w} = -Pr\ \alpha^2 g(t)\, Ra\ \phi + Pr\ (\mathrm{D}^2 - \alpha^2)^2 w \tag{2.6}$$

$$\dot{\phi} = (\mathrm{D}^2 - \alpha^2)\phi + w \tag{2.7}$$

where $g(t) = g_o + g_1 \cos \Omega t$, $g_o = g_o^*/g_c$, $g_1 = g_1^*/g_c$, $g_c = 9.80665\,\mathrm{m\,s^{-2}}$†, $\alpha^2 = \alpha_1^2 + \alpha_2^2$, $\Omega = \Omega^* \mathfrak{D}/d^2$, D denotes $\partial/\partial x_3$, and the overdot represents the time derivative, $\mathrm{d}/\mathrm{d}t$.

Rigid and conductive conditions are imposed on the disturbance velocity and

† Standard value of acceleration, see for example Mohr & Taylor (2000).

https://doi.org/10.1017/S0022112001003603 Published online by Cambridge University Press

temperature at $x_3 = 0$:

$$w = 0, \quad \mathrm{D}w = 0, \quad \phi = 0 \tag{2.8a–c}$$

At $x_3 = 1$, a flat non-deforming free surface yields

$$w = 0, \tag{2.9a}$$

while the tangential stress balance is given by

$$\mathrm{D}^2 w = -\alpha^2 Ma\phi. \tag{2.9b}$$

The disturbance flux condition at the free surface is

$$\mathrm{D}\phi + Bi\ \phi = 0. \tag{2.9c}$$

The resulting dimensionless parameters from the above equations are: the Prandtl number, $Pr = \nu/\mathfrak{D}$, thermal Rayleigh number, $Ra = g_c \beta \Delta \bar{T}^* d^3/\mathfrak{D}\nu$, thermal Marangoni number, $Ma = \gamma \Delta \bar{T}^* d/\mathfrak{D}\mu$, and surface Biot number, $Bi = h_1 d/\kappa$.†

The disturbance equations are reduced to a set of $2N - 6$ ordinary differential equations, ODEs, using a spectral (Chebyshev) collocation scheme where N is the number of collocation points. A Floquet analysis is applied to examine the stability of the system of ODEs (Meirovitch 1988; Joseph 1976). The monodromy matrix is computed by integrating the set of ODEs $2N - 6$ times over the period τ. Floquet multipliers, ρ_j, which are the eigenvalues of the monodromy matrix are then computed, and the characteristic exponents, λ_j, which determine the stability of the system are related to the floquet multipliers as $\lambda_j = (1/T)\ln(\rho_j)$. The characteristic exponent with the largest $\mathrm{Re}(\lambda)$, determines the stability of the system. If $\mathrm{Re}(\lambda)$ is positive, disturbances grow, if $\mathrm{Re}(\lambda)$ is negative, disturbances decay. The imaginary part of λ is multivalued and characterizes the system response. The response is synchronous when $\mathrm{Im}(\lambda) = n\Omega$, and subharmonic when $\mathrm{Im}(\lambda) = (n + \frac{1}{2})\Omega$, where n is an integer value. When the two frequencies are incommensurate, $|\delta| \neq n$ for $\mathrm{Im}(\lambda) = \delta \frac{1}{2}\Omega$, the response is quasi-periodic (Gresho & Sani 1970; Joseph 1976; Saunders *et al.* 1992; Terrones & Chen 1993).

Results from the Floquet-collocation scheme were verified in part by comparison to the exact solution of the unmodulated Marangoni–Bénard problem,

$$Ma = \frac{8\alpha^2 \cosh\alpha(\alpha - \sinh\alpha\cosh\alpha)}{(\alpha^3 \cosh\alpha - \sinh^3\alpha)}, \tag{2.10}$$

obtained by Pearson (1958). The unmodulated problem is autonomous, therefore the system of equations can be viewed as periodic over an arbitrary period, τ, in the context of a Floquet analysis. Similar validation strategies have been applied in the examination of modulated Rayleigh–Bénard type (double-diffusive/soret) systems (Saunders *et al.* 1992; Terrones & Chen 1993). For this study, ten collocation points were sufficient to give five- and six-digit agreement with the exact solution, while twelve collocation points provided six to seven digit agreement. Spatial resolution (number of collocation points) was varied to assess convergence behaviour at finite modulation amplitudes. Results from ten collocation points provided four- to five-digit agreement with those of 20 collocation points, while twelve collocation points gave five-digit agreement or better over the parameter ranges investigated. Results presented in § 3 were obtained primarily using $N = 10$, and in the other cases using

† The quantity, $h_1 d/\kappa$, is also referred to as the surface Nusselt number in the literature. h_1 is the surface heat transfer coefficient defined in Pearson (1958) and Skarda, Jacqmin & McCaughan (1998) (among several references). κ is the thermal conductivity of the fluid layer.

https://doi.org/10.1017/S0022112001003603 Published online by Cambridge University Press

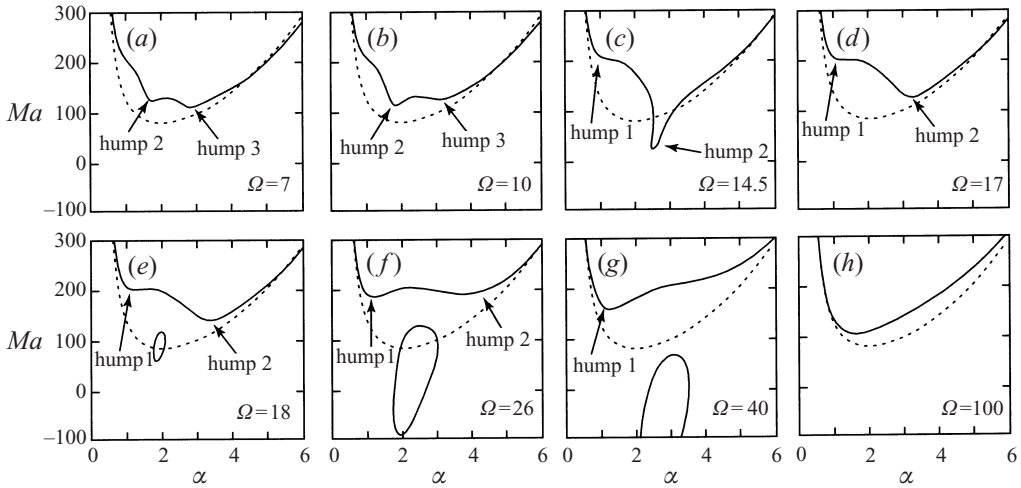


FIGURE 1. Neutral stability curves for $Pr = 1$, $Bi = 0$, $g_0 = 0$, $g_1 Ra = 5000$: ——, modulated neutral stability; - - -, unmodulated neutral stability.

$N = 12$. The problem was also formulated using a traditional Galerkin scheme, primarily to carry out the one-term computations in § 4. However, calculations using five to six trial functions were performed to further check our spectral computations.

3. Results

3.1. *Neutral stability boundaries in* (α, Ma)*-space*

The effect of modulation frequency on neutral stability is first examined in (α, Ma)-space, which has traditionally been used to study stability behaviour for the unmodulated Marangoni–Bénard problem. The set of neutral stability curves in figures 1(*a*) to 1(*h*) corresponds to Pr and $g_1 Ra$ values of 1 and 5000, respectively, and the classical Marangoni–Bénard condition of an insulated free surface, $Bi \to 0$, is applied at the upper boundary. Below each curve, the system is stable and 'small' disturbances decay, while above the curve, the system is unstable and the disturbances will grow in time. The unmodulated neutral stability curve is also shown in each figure for direct comparison with modulated neutral stability boundaries.

Figure 1(*a*) reveals the existence of two small local minima (denoted as humps) near the bottom of the neutral stability curve for $\Omega = 7$. Ma_c is associated with hump 3 in figure 1(*a*) and shifts to hump 2 for $\Omega = 10$ in figure 1(*b*). This suggests that a double minimum exists along the synchronous curve for some Ω between 7 and 10. In figure 1(*c*) where $\Omega = 14.5$, hump 2 forms a narrow finger that extends below the unmodulated Ma_c of 79.6, thus having a destabilizing effect on the unmodulated neutral stability curve. Another local minimum, hump 1, is found near $\alpha = 1$ in figure 1(*c*). Examination of figure 1(*d–f*) indicates hump 1 becomes more prominent as hump 2 recedes with increasing Ω, suggesting the presence of another double minimum. Hump 2 eventually disappears with increasing modulation frequency. Between Ω of 17 and 18, a subharmonic closed neutral stability branch forms. This region of instability grows with increasing modulation frequency until reaching an Ω of approximately 35. The subharmonic branch then begins to shrink and shifts to higher wavenumbers and lower Marangoni numbers, and eventually disappears as Ω

https://doi.org/10.1017/S0022112001003603 Published online by Cambridge University Press

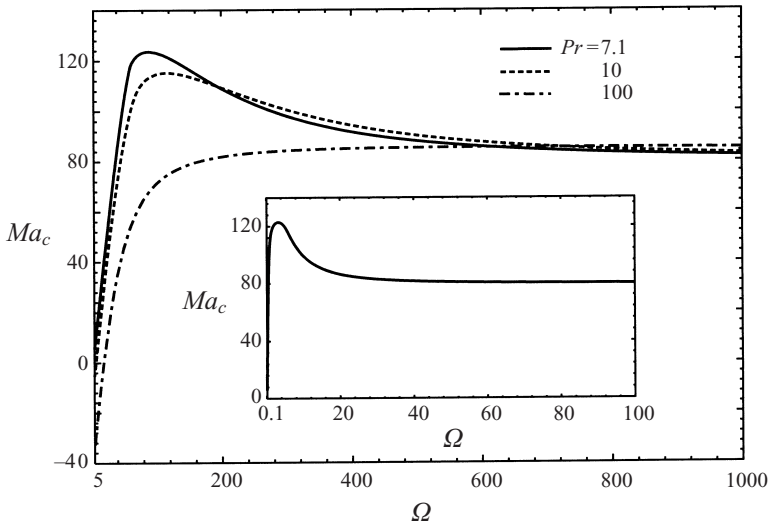


FIGURE 2. Ma_c versus Ω for the synchronous branch at different values of Pr. $g_0 = 0$, $g_1 Ra = 5000$. Inset shows critical curve for $Pr = 0.01$.

increases to a value of 100 where only the synchronous branch is evident. For $\Omega \geqslant 100$ the subharmonic loop shifts out of the range of Ma values explored while modulation is observed to have a stabilizing effect on the synchronous branch. The stabilization effect however diminishes with further increase of the modulation frequency.

The behaviour of critical Marangoni numbers, Ma_c, and critical wavenumbers, α_c, with respect to modulation frequency are shown in figures 2 and 3 for Pr values of 0.01, 7.1, 10 and 100. In view of the complex topology of the neutral stability curves, the critical values for $Pr = 1$ are presented separately in figure 4. This level of complexity, specifically multiple minima and subharmonic modes, was not observed in the neutral stability plots at the other Pr values we investigated. The absence of subharmonic behaviour for Pr values away from 1 may be due in part to larger damping with respect to $Pr = 1$. As described in § 3.2, larger modulation amplitudes are then required to achieve alternating subharmonic and synchronous instability behaviour. On the other hand, the $Pr = 1$ results shown in figures 1 and 4 indicate that the modulation amplitude, $g_1 Ra = 5000$, is sufficient to reach a subharmonic resonant mode which is also consistent with results in § 3.2.

Figure 2 shows that gravity modulation for sufficiently small Ω is destabilizing for all Pr values investigated. As Ω increases, gravity modulation has a stabilizing effect on Ma_c which reaches a maximum at some finite values of Ω. The stabilizing effect then decreases with a further increase in Ω, and approaches the unmodulated critical value of $Ma_{cp} = 79.607$ as $\Omega \to \infty$. The unmodulated critical wavenumber is $\alpha_{cp} = 1.993$. The subscript cp denotes the critical value of the unmodulated problem originally formulated by Pearson (1958). Values of Ma_c, Ω, and α_c where maximum stabilization occurs are given in table 1.

Critical and extremum values of Ma and α for $Pr = 1$ are shown in figure 4. Critical Marangoni numbers and corresponding wavenumbers for both synchronous and subharmonic branches are observed. Three local minima of the synchronous branch and their dependence on modulation frequency are also shown in figure 4. The corresponding α_c, displayed in the inset, show that these minima are associated with relatively large wavenumber differences, where cell sizes can differ by factors

https://doi.org/10.1017/S0022112001003603 Published online by Cambridge University Press

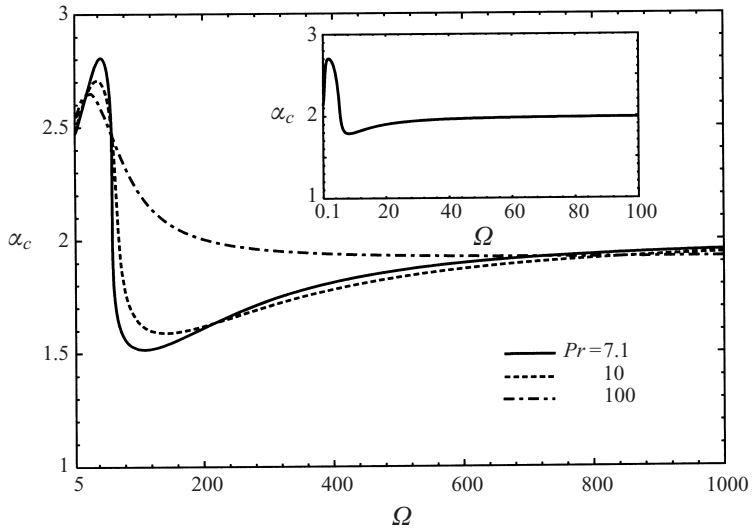


FIGURE 3. As figure 2 but for α_c. Inset shows critical curve for $Pr = 1$.

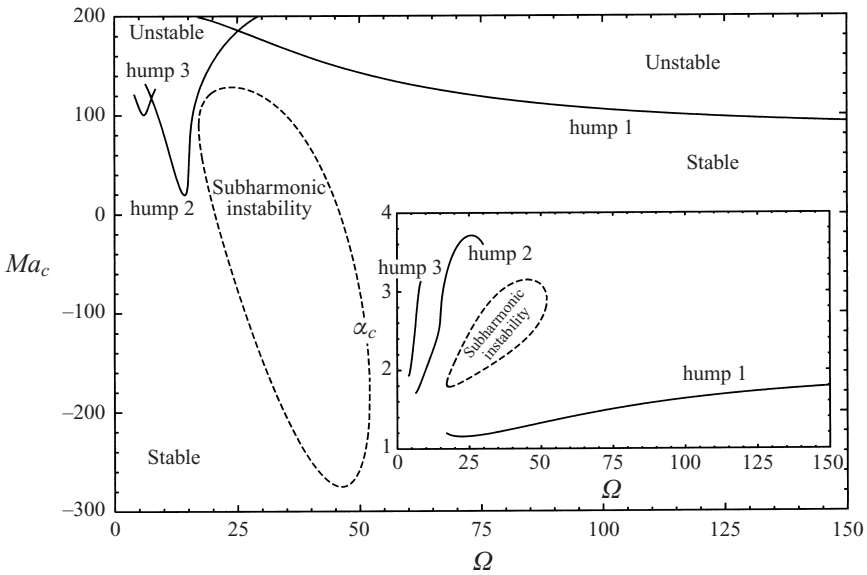


FIGURE 4. Ma_c versus Ω. $Pr = 1$, $g_0 = 0$, $g_1 Ra = 5000$. Solid lines denote the synchronous mode, and the dotted line denotes the subharmonic mode. The lower Ma value on the subharmonic loop, for given Ω, is Ma_c (the upper Ma values on the loop are maxima). The inset shows corresponding α_c values.

of two to three. This is also confirmed upon examining the location of the humps in figure 1. For convenience, these locations and the critical values corresponding to the two double minima (intersection points) observed in figure 4 are given in table 2. Physically, the double minima suggest the possible occurrence of mode switching where the cellular (or roll) pattern alternates between two cell (or roll) sizes dictated by the two different wavenumbers. Such a process would be easily observed given the large difference in the two wavenumbers associated with each of the double minima

https://doi.org/10.1017/S0022112001003603 Published online by Cambridge University Press

Pr	g_1Ra	Ω	Ma_c	α_c
0.01	5000	3.4	125.77	2.68
7.10	5000	88.0	123.67	1.54
10.00	5000	116.0	115.20	1.60
100.00*	5000	1000.0*	85.09*	1.92*

* Maximum stabilization occurs beyond $\Omega = 1000$.

TABLE 1. Values of Ω, Ma_c, and α_c for maximum stabilization

Ω	Ma_c	α_{c1}	α_{c2}
9.00	124.0	1.7	3.1
25.24	185.7	1.2	3.5

TABLE 2. Location and critical values for double minima

in table 2. Figure 4 also reveals that the subharmonic branch forms at Ω slightly less than 17.5 and disappears just beyond Ω of 52. The subharmonic instability extends to Ma values less than -250, where a stable temperature gradient occurs for the unmodulated problem.

3.2. *Modulated Marangoni–Bénard instabilities in* $(1/\Omega, g_1Ra)$*-space*

For the unmodulated system, the neutral stability behaviour of the Marangoni–Bénard and Rayleigh–Bénard problem is qualitatively similar when comparing results in (α, Ma)-space to those in (α, Ra)-space. For the modulated problem, correspondence of stability behaviour between (α, Ma)-space and (α, Ra)-space is complicated by the fact that changing Ra simultaneously affects both the steady instability agent (buoyancy) and the modulation amplitude which is also part of the buoyancy term. In contrast, varying Ma only affects a steady instability agent, which in this case is the variation of surface tension along the free surface. One alternative is to consider gravity modulation effects in $(1/\Omega, g_1Ra)$-space to facilitate comparisons between the Marangoni–Bénard and Rayleigh–Bénard problems.

It is quite impractical to characterize the stability behaviour in the full parameter space for the (linear but non-autonomous) problem. Identification of stability boundaries in $(1/\Omega, g_1Ra)$ provides a direct means of assessing modulation effects. In this section, stability boundaries in $(1/\Omega, g_1Ra)$-space are used to quantify the effects of modulation frequency and amplitude for given values of (unmodulated) system parameters. Stability behaviour has been investigated in this manner in the pioneering works of Gershuni & Zhukhovitskii (1963) and Gershuni *et al.* (1970), and the recent detailed treatments of solutal and double-diffusive instabilities by Saunders *et al.* (1992), Murray *et al.* (1991) and Terrones & Chen (1993). In figures 5 to 7 and 10 to 12, sets of neutral stability maps in $(1/\Omega, g_1Ra)$-space are shown that correspond to different values of Pr, Ma, Ra, and g_0. We note that the problem depends on g_0Ra and g_1Ra rather than g_0, g_1, and Ra, separately.

A sequence of stability boundaries in $(1/\Omega, g_1Ra)$-space is shown in figures 5(a) to 5(l) for $Pr = 1$. The value of Ma increases for each snapshot (graph) in the figure 5 set, proceeding from (a) to (l). The wavenumber, α_0, is set to 2, approximately the critical wavenumber for the unmodulated Marangoni–Bénard problem. This choice of wavenumber is consistent with those chosen for the modulated Rayleigh–Bénard

https://doi.org/10.1017/S0022112001003603 Published online by Cambridge University Press

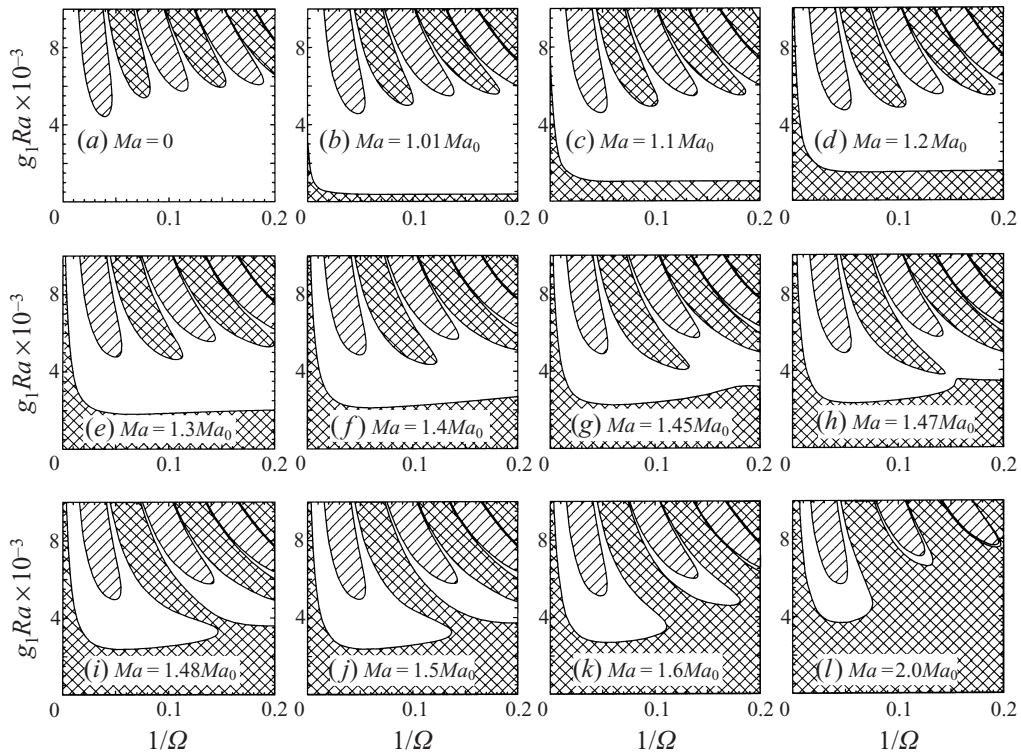


FIGURE 5. Sequence of stability boundaries in $(1/\Omega, g_1Ra)$ space for varying Ma. $Pr=1$, $Bi=0$, $\alpha=2$, $g_0=0$, $Ma_0=79.607$: hatched, subharmonic response; cross-hatched, synchronous response.

studies (Gershuni *et al.* 1970; Murray *et al.* 1991; Saunders *et al.* 1992). Since only a single α is considered, minima from such parameter space represent approximate critical values at best. As figures 3 and 4 indicate that critical wavenumbers for the modulated problem occur over a broader range of α, other values of α also merit exploration.

In figure 5(*a*), the steady acceleration level is $g_0=0$, corresponding to a zero gravity condition, and $Ma=0$ as well. Therefore both steady instability agents, buoyancy and surface tension variation, are zero. Alternating tongues of subharmonic and synchronous instability are observed in figure 5(*a*) for sufficiently large modulation amplitudes, g_1Ra. As modulation amplitude increases and modulation frequency decreases, the stable regions separating the subharmonic and synchronous instability tongues become quite thin. The minimum amplitude required to incite instability is $g_1Ra=4.426\times10^3$ and occurs for a modulation frequency of $\Omega=24.5$. Above this minimum amplitude a subharmonic instability develops. The results of figure 5(*a*) also bear a striking resemblance to the Rayleigh–Bénard results presented in Gershuni & Zhukhovitskii (1976) and Saunders *et al.* (1992) for $g_0=0$. This is not surprising since the principal difference with $Ma=0$ is then the application of Rayleigh's boundary conditions in previous studies as compared to the conditions given in § 1 for the present study. In fact, the stability boundaries for rectangular modulation, presented in the earlier works of Gershuni & Zhukhovitskii (1963) are also quite similar in appearance to those of figure 5(*a*) and aforementioned references where sinusoidal modulation is applied.

A region of instability develops for small modulation amplitudes when Ma exceeds

https://doi.org/10.1017/S0022112001003603 Published online by Cambridge University Press

Ma/Ma_0	$g_1 Ra_{min} \times 10^{-3}$	Ω
0.0	4.426	24.5
1.1	4.609	20.0
1.2	4.679	19.9
1.3	4.764	19.8
1.4	4.864	19.8
1.5	4.977	19.9
1.6	5.107	20.1
2.0	5.727	21.4

TABLE 3. Minimum amplitude ($g_1 Ra$) and forcing frequency of first subharmonic tongue

Ma_0 where $Ma_0 = 79.607$. For example, when $Ma = 1.01 Ma_0$, a very thin region of instability is observed at the bottom of figure 5(*b*). Gershuni *et al.* (1970) referred to the lowermost region of instability as the fundamental instability region and showed that it existed for Ra values exceeding the unmodulated neutral Ra value. (The situation equally applies to the Marangoni–Bénard problem where Ma values replace Ra values.) Increasing the modulation amplitude, $g_1 Ra$, suppresses the fundamental instability. As the modulation amplitude is further increased, regions of alternating subharmonic and synchronous instability are eventually reached. The modulation amplitude necessary to suppress the fundamental instability increases for larger values of Ma as observed in figures 5(*b–g*).

There are some characteristics of the alternating subharmonic/synchronous tongues† which appear to be unique to the modulated Marangoni–Bénard problem, not the Rayleigh–Bénard problem (see also § 3.3). Comparison of the snapshots (*a–h*) reveals that the synchronous fingers grow with increasing Ma. For a sufficiently large Ma value, the synchronous tongues extend to lower $g_1 Ra$ than the subharmonic tongues. The lowest modulation amplitude to incite instability occurs in the first subharmonic finger when $Ma \leqslant 1.2 Ma_0$, while the second tongue (synchronous) holds the minimum amplitude threshold for Ma values in the interval $1.3 Ma_0 \leqslant Ma \leqslant 1.47 Ma_0$. Upon further increasing Ma, the region of fundamental instability and the synchronous instability tongues merge and surround the subharmonic tongues. The value of Ma where the synchronous tongues and fundamental instability region initially meet occurs for Ma in the range $1.47 Ma_0 \leqslant Ma \leqslant 1.48 Ma_0$. Beyond $1.48 Ma_0$, the fundamental instability region and the synchronous tongues are indistinguishable, and the stable regions surrounding the subharmonic instability regions continue to shrink. Careful inspection of figure 5(*a–l*) also reveals that the subharmonic tongues recede with increasing Ma although this occurs much more slowly than the growth of the synchronous tongues. The minimum amplitudes required to excite a subharmonic instability in the figure 5 snapshots, and their associated Ω are given in table 3. These amplitudes were always associated with the first subharmonic region (that of largest modulation frequency).

The stability results shown in figure 6 are for $Pr = 10$. In contrast to the figure 5 results, the increased mechanical damping for $Pr = 10$ is responsible for the significantly larger modulation amplitude required to achieve subharmonic instability. For example in figure 6(*a*) this minimum amplitude is $g_1 Ra \approx 20 \times 10^3$, while $g_1 Ra \approx 4.4 \times 10^3$ for the corresponding $Pr = 1$ in figure 5(*a*). In figure 6(*a*) where no fundamental

† The instability tongues are also referred to as instability regions, intervals, or bands (cf. Gershuni & Zhukhovitskii 1976 and Saunders *et al.* 1992).

https://doi.org/10.1017/S0022112001003603 Published online by Cambridge University Press

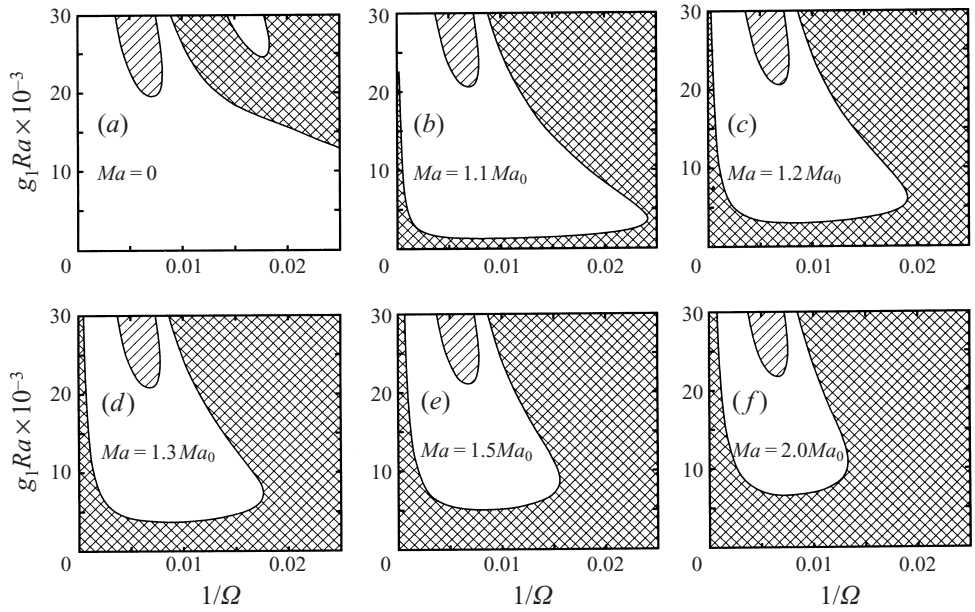


FIGURE 6. As figure 5 but for $Pr = 10$.

instability exists, the modulation amplitude for the synchronous instability boundary continues to decrease with decreasing Ω. A stable tongue is observed within this unstable region. The synchronous instability resonance is excited at smaller modulation amplitudes than the subharmonic instabilities tongue but these occur at low modulation frequencies. The larger Pr value also results in the subharmonic/synchronous instability regions being shifted to higher Ω. However, this shift appears largely due to choice of scaling for Ω and is further discussed in § 4.3.

For $Ma = 1.2Ma_0$ (figure 6*b*) the fundamental instability region is again present as in the case of $Pr = 1$ (figure 5*d*). However, the fundamental instability region is observed to be slightly thicker in figure 6(*b*) than for the same Ma value in the case of $Pr = 1$. This is also attributed to the increase in damping due to viscous dissipation. No distinction between the fundamental instability region and synchronous tongues of instability is observed in the figure 6 snapshots. The separation of the two boundaries apparently occurs at smaller Ma values than we have considered, within the range $1.1Ma_0 < Ma < 1.2Ma_0$. This is in contrast to the $Pr = 1$ results where the merging of synchronous tongues and the fundamental instability boundary did not occur until $Ma > 1.47Ma_0$. The stable tongue observed in figure 6(*a*) for $Ma = 0$ has moved beyond the range of g_1Ra values considered, for all other Ma values (cf. figure 6*b–f*). Careful inspection of figure 6 also reveals that the subharmonic instability tongue recedes, while the stable region surrounding the subharmonic tongue shrinks with increasing Ma, similar to the $Pr = 1$ results.

The $Pr = 0.01$ results in figure 7 also shift the instability tongues to small Ω, which as noted above, is also due in part to our choice of frequency or time scale. For $Ma < 1.5Ma_0$, the leftmost subharmonic tongue ($1/\Omega \approx 0.2$) reaches a smaller modulation amplitude (g_1Ra) than the other tongues to the right. However, for $Ma = 1.5Ma_0$ in figure 7(*e*), the leftmost synchronous tongue ($1/\Omega \approx 0.5$) contains the minimum g_1Ra value. This synchronous tongue appears to merge with the fundamental instability region in figure 7(*f*) (just beyond the $1/\Omega$ range we examined).

https://doi.org/10.1017/S0022112001003603 Published online by Cambridge University Press

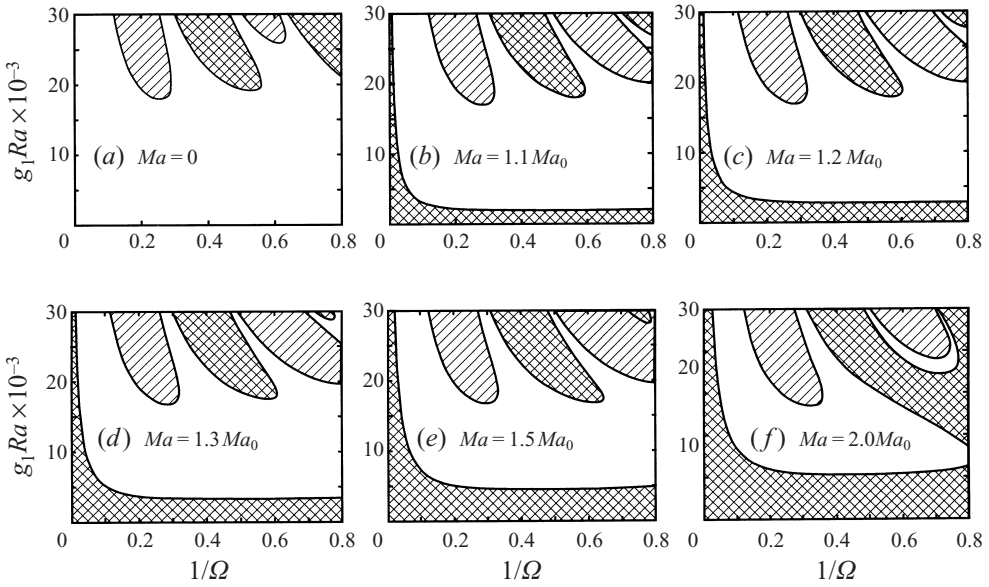


FIGURE 7. As figure 5 but for $Pr = 0.01$.

The overall behaviour of the subharmonic and synchronous tongues with increasing Ma, in figure 7, is consistent with that described for $Pr = 1$ case. For the case of very small Pr, $Pr = 0.01$, subharmonic and synchronous instability tongues shown in figure 7 are at higher modulation amplitudes than for $Pr = 1$ results. Since Pr is small, large damping of the system is caused through thermal diffusion. As opposed to representing an absolute measure of damping, here, Pr is a measure of relative damping, viscous dissipation to thermal diffusion. Stability boundaries of figure 5 to 7 in conjunction with the results for Pr values of 1 and 10 suggest that a minimum modulation amplitude exists for some finite value of Pr, in the range $0.01 < Pr < 10$, which qualitatively agrees with Gershuni & Zhukhovitskii (1963, 1976). Using a highly truncated, one-term Galerkin approximation, they found that minimum damping occurred for $Pr = 1$ in their modulated Rayleigh–Bénard problem. These damping aspects do not appear to have received further attention in subsequent spectral and higher-order studies of modulated Rayleigh–Bénard problems and are considered below.

The variation of the critical Marangoni number, η_{Ma_c}, associated with the fundamental instability boundary is shown in figures 8 and 9 as a function of modulation amplitude. The variation, η_{Ma_c}, is the change in Ma_c with respect to the unmodulated critical Ma value, Ma_{cp} and is defined as $(Ma_c - Ma_{cp})/Ma_{cp}$. Each of the critical value curves shown in the figures corresponds to a different Pr value in the range, $0.001 \leqslant Pr \leqslant 500$. Results in figures 8 and 9 correspond to Pr/Ω^2 values of $1/(25)^2$ and $1/(50)^2$, respectively. For convenience, Ra is set to 1000 and the relative amplitude, g_1 (as defined by Gershuni & Zhukhovitskii 1963) is represented on the abscissa. Wavenumbers associated with Ma_c are shown in the insets of figures 8 and 9. The critical wavenumber, α_c decreases with modulation amplitude for all cases except $Pr = 0.01$ and $Pr = 0.001$. For Pr values 0.001 and 0.01, α_c increases with modulation amplitude. The departure from α_{cp} is small for $g_1Ra < 1000$, but quickly grows as g_1Ra increases beyond 10^3.

A reasonable approximation based on the results from both figures is that the

https://doi.org/10.1017/S0022112001003603 Published online by Cambridge University Press

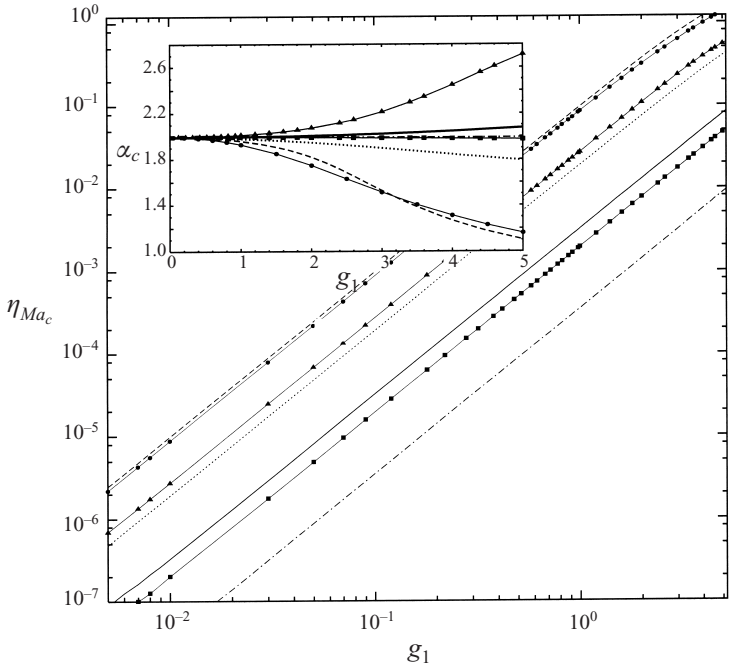


FIGURE 8. Effect of relative amplitude g_1 on fundamental instability boundary for different values of Pr. $Ra = 1000$, $g_0 = 0$, $Pr/\Omega^2 = 1/(25)^2$ ——, $Pr = 0.001$; —▲—, $Pr = 0.01$; - - -, $Pr = 0.1$; —●—, $Pr = 1.0$; ·····, $Pr = 10$; —■— $Pr = 100$; –·–·–, $Pr = 500$.

variation of Ma_c, η_{Ma_c} increases with square of the modulation amplitude, $g_1 Ra$. More precisely for $g_1 Ra < 1000$, $\eta_{Ma_c} \propto (g_1 Ra \times 10^{-3})^{1.99}$, where the proportionality constant is a function of Pr. For a given g_1 value in figure 8, η_{Ma} displays an $O(100)$ variation due to the Pr dependence. The greatest variation in Ma_c occurs for $Pr = 0.1$ while the $Pr = 500$ results display the most insensivity to modulation due to large viscous damping. These results further support the existence of a minimum Pr as noted above. However, results of figures 8 and 9 suggest that the value of Pr associated with minimum damping occurs at a Pr slightly less than 1, in the range $0.01 < Pr < 1$, rather than $Pr = 1$ computed for the modulated Rayleigh–Bénard problem (Gershuni & Zhukhovitskii 1963). While the existence of a minimum Pr value is confirmed, it is unclear whether the difference in these results and Gershuni & Zhukhovitskii's is due to different steady driving forces (surface tension variation vs. buoyancy) or the result of the one-term approximation applied by Gershuni & Zhukhovitskii (1963, 1976). In general, the variation in Ma_c, η_{Ma_c} associated with the fundamental instability region is small for $g_1 < 0.1$. Modulation effects are suppressed until larger g_1 values ($g_1 \approx 1$) for very small or very large Pr. For moderate Pr values, Ma_c variations of 0.1% and larger are observed at $g_1 > 0.1$.

While a minimum modulation amplitude, $(g_1 Ra)_c$, is observed along the fundamental instability boundary, the boundary is shown to be relatively flat near $(g_1 Ra)_c$ in figures 5 to 7. When η_{Ma} is sufficiently small that the fundamental instability region and the synchronous tongues remain separated, as in figures 5(a–e) and 7(b–e), critical $g_1 Ra$ values obtained from figures 8 and 9 approximate reasonably the fundamental instability boundary for other modulation frequencies, $\Omega < \Omega_c$, for the ranges of Ω investigated in this paper.

https://doi.org/10.1017/S0022112001003603 Published online by Cambridge University Press

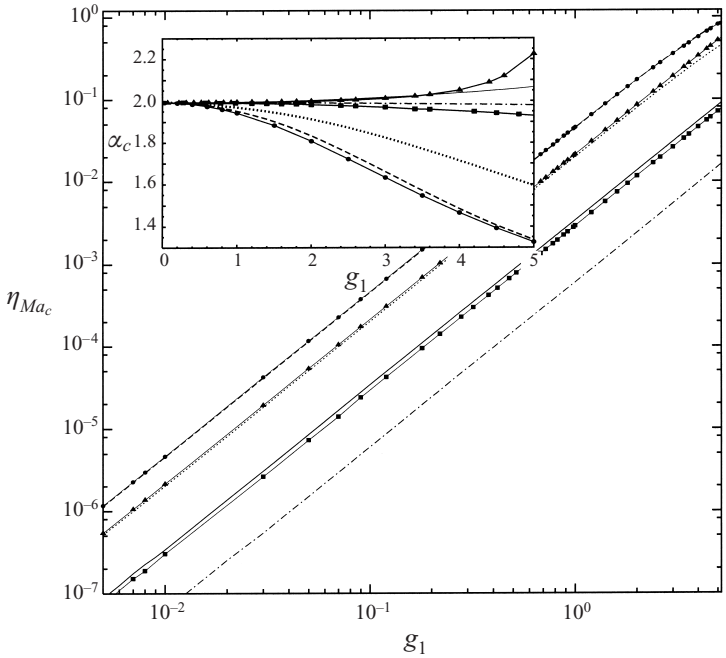


FIGURE 9. As figure 8 but for $Pr/\Omega^2 = 1/(50)^2$.

3.3. *Modulated Rayleigh–Bénard results*

The modulated Rayleigh–Bénard problem is briefly considered, to examine some factors that might contribute to the differences (with respect to the modulated Marangoni–Bénard problem) that were noted in § 3.2. Results that follow in figures 10 and 11 correspond to the modulated Rayleigh–Bénard problem with a rigid conductive lower surface and a free insulated upper surface ($Bi = 0$). Surface tension effects are also eliminated ($Ma = 0$) for both sets of results. The difference between this problem and that considered by Gershuni & Zhukhovitskii (1963) is the differing boundary conditions. Gershuni & Zhukhovitskii considered the upper and lower surfaces as free and conductive boundaries as opposed to those in equations (3.8) and (3.9) used for this study. The modulated double-diffusive study of Saunders *et al.* (1992) also allows limited comparison with their results, specifically their stationary stability boundaries. For the stability boundaries shown in figures 10 the steady gravity acceleration level, g_0, is set to one, corresponding to terrestrial conditions, and the value of Ra differs, increasing from snapshot (*a*) to snapshot (*h*). On the other hand, for results of figure 11, Ra is fixed to Ra_0 while g_0 increases in each snapshot from (*a*) to (*h*).

As in the case of non-zero Ma, a fundamental instability occurs for $Ra > Ra_0$ which is stabilized for some finite modulation amplitude. Here, α_0 is again set to 2 and the corresponding Ra_0 is 670.280.† Further increase in $g_1 Ra$ eventually destabilizes the layer. In general, alternating bands of synchronous and subharmonic instability separated by thin stable regions are observed, which is characteristic of gravity modulation Rayleigh–Bénard results of Gershuni & Zhukhovitskii (1963). The stability boundaries for $Ra = 1.01Ra_0$ in figure 10(*a*) are similar to those in figure 5(*a*) for $Ma = 1.01Ma_0$. However, unlike the non-zero Ma results of figure 5, the modulated

† Analogously to the Ma case, these values are quite close to α_c and Ra_c values, 2.096 and 669.00, respectively.

https://doi.org/10.1017/S0022112001003603 Published online by Cambridge University Press

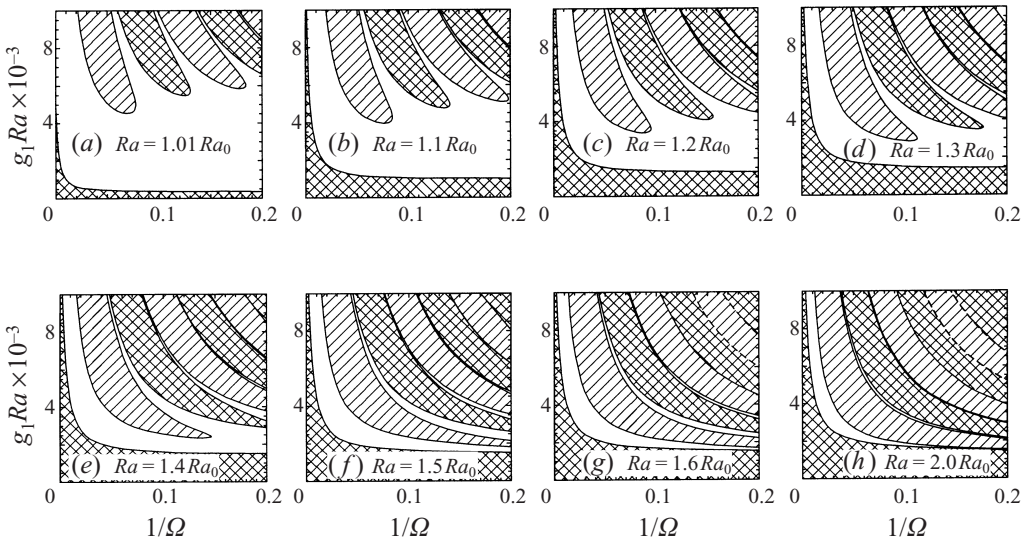


FIGURE 10. Sequence of stability boundaries in $(1/\Omega, g_1 Ra)$ space for varying Ra. $Pr = 1$, $Bi = 0$, $Ma = 0$, $\alpha = 2$, $g_0 = 1$, $Ra_0 = 670.29$: hatched, subharmonic response; cross-hatched, synchronous response.

Rayleigh–Bénard results of figure 10 show that both subharmonic and synchronous instability regions elongate and tend to lower modulation amplitudes with increasing values of Ra. Even at the larger Ra values, the stability bands remain well defined for the modulated Rayleigh–Bénard results. The synchronous instability regions do not merge with the fundamental instability region as was the case for the modulated Marangoni–Bénard results of the previous section.

Results in the form of $(1/\Omega, g_1 Ra)$ stability boundaries for the modulated Rayleigh–Bénard problem are somewhat limited. However, a set of $(1/\Omega, g_1 Ra)$ stability boundaries for three different Ra values shown in Gershuni & Zhukhovitskii (1963) provide a basis for comparison. These results are also found in more recent work, Gershuni & Zhukhovitskii (1976). Although these specific sets of results are based on a one-term Kantorovich (Galerkin) model, they have been shown to be in good agreement with higher-order calculations of the equivalent problem. Figure 10 stability boundaries show very similar behaviour to their results, with the principal difference between the two works being the choice of boundary conditions as describe above. Similar behaviour is observed with some of Saunders *et al.*'s (1992) stationary stability results. This simple alteration of the boundary conditions is not responsible for the differences observed (merging of the fundamental instability and synchronous boundaries, and receding subharmonic) between the modulated Marangoni–Bénard and Rayleigh–Bénard problem. The boundary condition differences quantitatively change the stability boundaries, but there remains a strong qualitative resemblance between the two results.

Varying Ra simultaneously changes both the steady instability term and the modulation amplitude, which is precisely the effect examined in figure 10. On the other hand, for the modulated Marangoni–Bénard problem, varying Ma (see figure 5) changes only the steady instability term. One way to make a more direct comparison with the stability boundaries of figure 5 might be to consider varying g_0 values. Incrementally changing gravity levels would probably be difficult and impractical to implement experimentally; however from the computational standpoint, it allows isolating and

https://doi.org/10.1017/S0022112001003603 Published online by Cambridge University Press

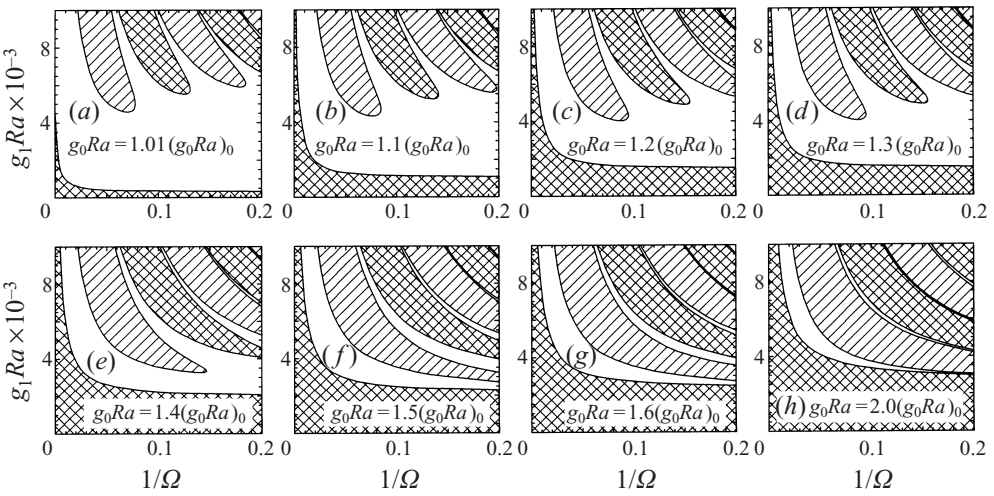


FIGURE 11. Sequence of stability boundaries in $(1/\Omega, g_1Ra)$ space for varying g_0Ra. $Pr=1$, $Bi=0$, $Ma=0$, $\alpha=2$: hatched, subharmonic response; cross-hatched, synchronous response.

comparing analogous effects of the steady stratifying agents, buoyancy and surface tension variation.

Stability boundaries in $(1/\Omega, g_1Ra)$ are shown in figure 11 for different g_0 values. These results are qualitatively similar to those of increasing Ra in figure 10, rather than the results of increasing Ma in the previous section (§ 3.2). On comparison, the fundamental instability boundary for increasing g_0 in figure 11 is observed to occur at larger amplitudes, g_1Ra, than for the case of increasing Ra. This is expected since increasing g_1Ra in figure 11 destabilizes the buoyancy term of the unmodulated system, while in figure 10 increasing Ra increases not only the steady term, but also the modulation amplitude which was observed to have a stabilizing effect on the system near Ra_0. Merging of the fundamental instability with the alternating synchronous bands was not observed in figures 10 and 11. Therefore, it seems likely that the merging behaviour is primarily associated with the location of the stratifying agency, surface tension variation, which is applied as a surface force rather than a body force as in the case of the buoyancy problem.

4. One-term approximations

Using a one-term Galerkin approximation, the gravity-modulated Marangoni–Bénard problem can be reduced to the Mathieu equation which in turn reduces the number of parameters from seven to three. A direct analogy can then be made to a well-studied mechanical system, a viscously damped pendulum that oscillates vertically at its fulcrum. This analogy was used by Gresho & Sani (1970) to study the modulated Rayleigh–Bénard problem, and is extended here to the combined Marangoni–Bénard/Rayleigh–Bénard problem.

4.1. *Mathieu equation development and mechanical analogies*

Substituting the trial solutions, $w^N(x_3,t)=\sum_{i=1}^{N}A_i(t)\hat{w}(x_3)$ and $\phi^N(x_3,t)=\sum_{i=1}^{N}B_i(t)\hat{\phi}(x_3)$, into equations (2.6) to (2.9*c*), leads to the following one-term result:

$$\begin{bmatrix} b_1 & 0 \\ 0 & b_2 \end{bmatrix}\begin{bmatrix} \dot{A} \\ \dot{B} \end{bmatrix}=\begin{bmatrix} a_{11} & a_{12} \\ a_{21} & a_{22} \end{bmatrix}\begin{bmatrix} A \\ B \end{bmatrix} \tag{4.1}$$

https://doi.org/10.1017/S0022112001003603 Published online by Cambridge University Press

where

$$b_1 = [(\mathrm{D}\hat{w}, \mathrm{D}\hat{w}) + \alpha^2(\hat{w}, \hat{w})], \qquad p_1 = [(\mathrm{D}^2\hat{w}, \mathrm{D}^2\hat{w}) + 2\alpha^2(\mathrm{D}\hat{w}, \mathrm{D}\hat{w}) + \alpha^4(\hat{w}, \hat{w})],$$
$$b_2 = (\hat{\phi}, \hat{\phi}), \qquad p_2 = \alpha^2(\hat{w}, \hat{\phi}),$$
$$a_{11} = -Pr\, p_1, \qquad p_3 = \alpha^2\phi(1)w(1),$$
$$a_{12} = Pr[g(t)Ra\, p_2 - Ma\, p_3], \qquad p_4 = [(\mathrm{D}\hat{\phi}, \mathrm{D}\hat{\phi}) + \alpha^2(\hat{\phi}, \hat{\phi})],$$
$$a_{21} = (\hat{w}, \hat{\phi}),$$
$$a_{22} = -p_4, \qquad g(t) = g_0 + g_1 \cos \Omega t.$$

The inner product is denoted by

$$(f, g) = \int_0^1 f(x_3)g(x_3)\mathrm{d}x_3.$$

Combining the first-order equations in (4.1) and re-scaling the dimensionless time, t, as $t = 2\tau/\Omega$, the pair of equations can be reformulated in terms of the damped Mathieu equation:

$$\ddot{B} + 2\varsigma\dot{B} + (\xi + 2q\cos 2\tau)B = 0 \tag{4.2}$$

where the overdot now represents, $\mathrm{d}/\mathrm{d}\tau$. The coefficients, ς, ξ, and q can be interpreted as effective damping, stiffness, and amplitude coefficients, respectively. The standard form of the Mathieu equation is $\ddot{y} + (a + 2q\cos 2\tau)y = 0$, where the coefficients a and q are the Mathieu coefficients (McLachlan 1964; Abramowitz & Stegun 1974). The coefficients ς, ξ, a, and q are then defined in terms of the seven fluid transport parameters:

$$\varsigma = \frac{1}{\Omega}\left(Pr\frac{p_1}{b_1} + \frac{p_4}{b_2}\right), \tag{4.3}$$

$$\xi = \frac{4Pr}{\Omega^2}\left(\frac{p_1\, p_4}{b_1\, b_2} - \frac{a_{21}\, p_2}{b_1\, b_2}g_0\, Ra - \frac{a_{21}\, p_3}{b_1\, b_2}\, Ma\right), \tag{4.4}$$

$$a = \varsigma - \xi^2, \tag{4.5}$$

$$q = -2\frac{a_{21}\, p_2}{b_1\, b_2}\,\frac{g_1\, Pr\, Ra}{\Omega^2}. \tag{4.6}$$

Therefore, we can reduce the gravity-modulated Rayleigh–Bénard/Marangoni–Bénard problem to (approximately) the Mathieu equation, for which tabulated and graphical solutions such as the Strutt diagram in figure 12 exist. The influence of the seven fluid transport parameters $(Pr, Ra, Ma, \alpha, g_0, g_1, \Omega)$ on stability can then be obtained by examining their relationship to the two Mathieu parameters and damping ratio. Subject to equations (4.3)to (4.6), modified growth rate diagrams similar to those constructed by Gresho & Sani (1970) remain valid for the present problem.

The velocity and temperature trial functions are employed:

$$\hat{w}_i(z) = (1 - z)z^2 + \frac{1}{\pi^2}\sin^2(\pi z), \tag{4.7}$$

$$\hat{\phi}(z) = \left(1 - \frac{z}{2}\right)z + \sin\left(\frac{\pi}{2}z\right). \tag{4.8}$$

With these trial functions, the one-term approximation was shown to give satisfactory quantitative accuracy for the unmodulated doubly diffusive instability (Skarda *et al.* 1998). An error assessment of the one-term Galerkin approximation for the unmodulated double-diffusive instability showed that predicted Ma_c values from the one-term

https://doi.org/10.1017/S0022112001003603 Published online by Cambridge University Press

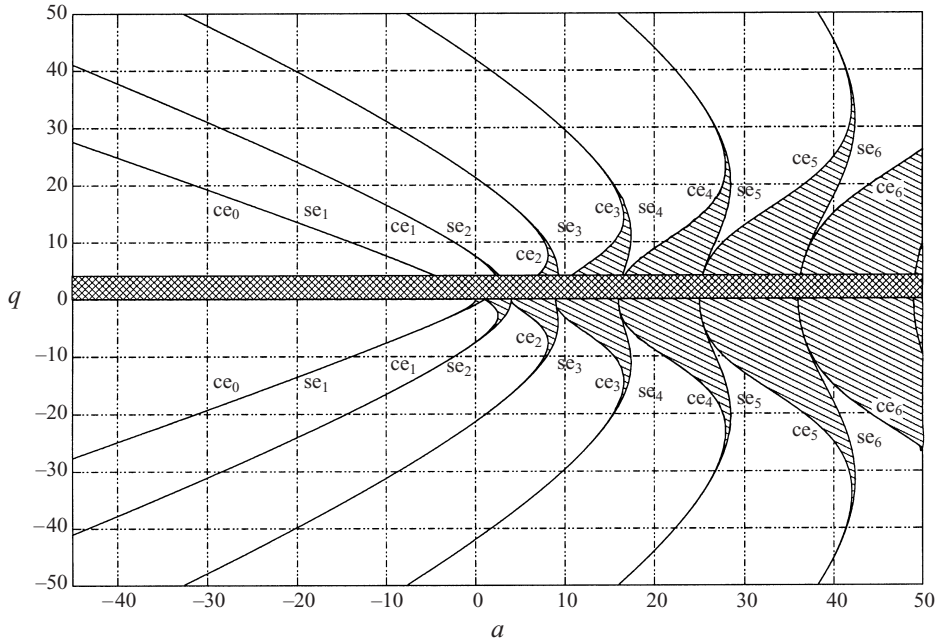


FIGURE 12. Alternating stable and unstable regions in parameter space for the Mathieu equation (Strutt diagram). Boundaries are the elliptic cosine, ce_i, and elliptic sine, se_i functions. Hatching denotes stable region. Cross-hatched region is the equivalent range for computed Gresho–Sani maps in figure 13.

approximation were within 10% to 20% of Ma_c values computed from the exact solution, while the one-term predictions of Ma_c for the Marangoni–Bénard problem and Ra_c for Raleigh-Benard problem are 10% lower and 6.8% higher, respectively, than corresponding collocation ($N = 10$) results.

4.2. *One-term results*

Gresho–Sani stability maps are given in figure 13(a, b) and have been computed for a larger range of a and q values to satisfy the range of values considered in this paper. Each curve in the contour plots is for constant values of $\zeta/\sqrt{\pm a}$. The + corresponds to the hanging pendulum while the − corresponds to the inverted pendulum. Since large variations in a and q occur over typical ranges of the transport parameters, the stability charts we constructed in figure 13(a, b) only cover a limited portion of this range. Values of q for $g_1 Pr\, Ra/\Omega^2 < 20$ are within this range, although values of both a and q can vary by several orders of magnitude for $Pr \gg 1$ for Ra and Ma values near neutral stability. Table 4 shows tabulated transport parameter values and the corresponding Mathieu parameters for selected one-term neutral stability results. These points are shown in figure 14(a–d) in (α, Ma)-space and in the corresponding Gresho–Sani map in figure 14(e).

Neutral stability curves generated from the one-term Galerkin approximation and the higher-order Chebyshev collocation scheme are shown in figure 14(a–d). Results are shown for Prandtl numbers of 0.01, 1, and 10. The one-term approximation is shown to be in good qualitative agreement with the higher-order results. The flattened appearance of the neutral stability curve in the region of Ma_c is observed on both one-term and collocation curves in figure 14(a). The critical wavenumber,

https://doi.org/10.1017/S0022112001003603 Published online by Cambridge University Press

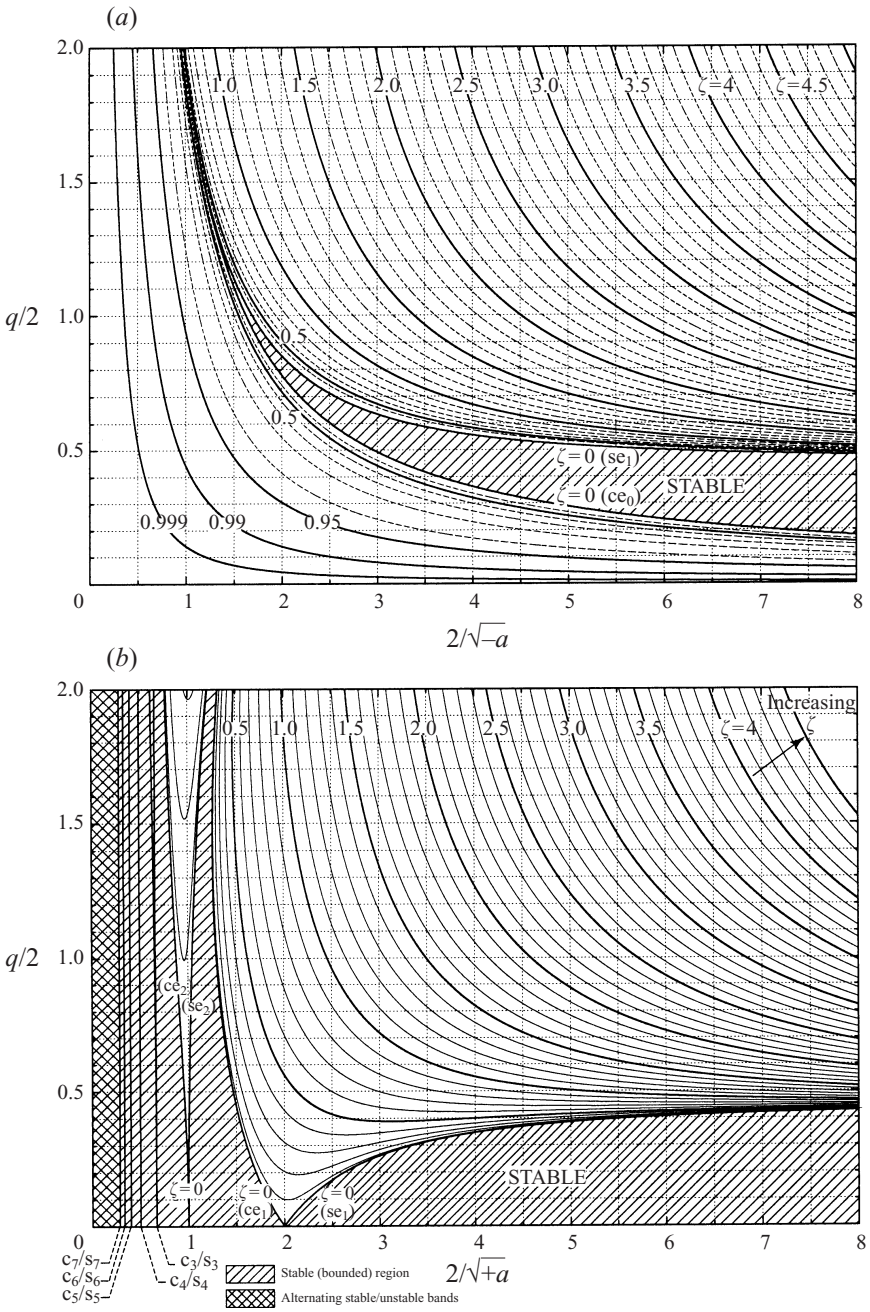


FIGURE 13. Gresho & Sani stability maps. (*a*) $a < 0$, (*b*) $a > 0$.

α_c, of approximately 3 is observed for both curves in figure 14(*a*). The synchronous curves of the one-term approximation are skewed to the left with respect to the unmodulated neutral stability curve in figures 14(*b*) and 14(*c*), which is consistent with the collocation curves. The one-term approximation predicts the occurrence of the subharmonic closed loop in figure 14(*b*), albeit in poor quantitative agreement with the higher-order collocation results. For a Prandtl number of 0.01, an error of

https://doi.org/10.1017/S0022112001003603 Published online by Cambridge University Press

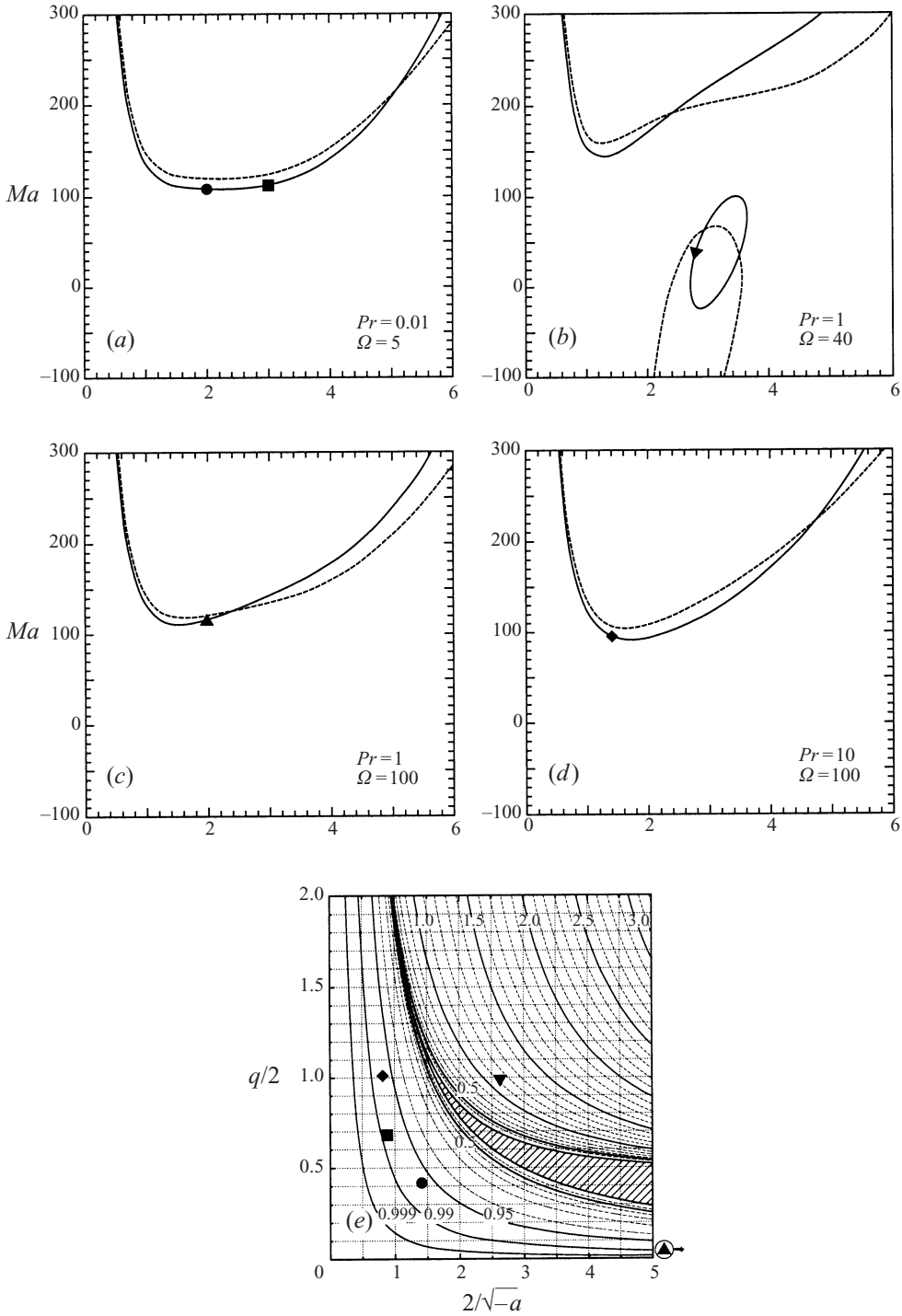


FIGURE 14. One-term neutral stability curves compared with higher order spectral results in (*a*) to (*d*), and Gresho–Sani map, (*e*), is indicated for table 4 data. $g_1 Ra = 5000$ and $g_0 = 0$. ——, one-term Galerkin approximation; - - - -, higher-order Chebyshev collocation.

https://doi.org/10.1017/S0022112001003603 Published online by Cambridge University Press

Pr	Ω	Ma	α	a	q	μ
0.01	5	108.363	2.0	−1.928	−0.819	1.339
0.01	5	112.353	3.0	−5.656	−1.399	2.346
1.00	40	2.280	2.703	−0.577	−1.932	0.863
1.00	100	96.718	2.0	−0.074	−0.115	0.261
10.00	100	112.018	1.4	−5.760	−2.049	2.330

TABLE 4. Tabulated values of one-term Galerkin results

3.8% to 11% is observed for wavenumbers between 1 and 3. Errors ranging between 1% and 20% are observed in one-term approximation values of Ma_c in figure 14(*b–d*).

In contrast, one-term approximation errors between 2% and 10% were obtained for the modulated Rayleigh–Bénard problem. At least three factors contribute to the larger one-term approximation errors in the case of the gravity-modulated Marangoni instability. First, trial functions are easily constructed for the Rayleigh–Bénard problem that satisfy all the boundary conditions, so that no error contributions occur at the boundaries. For the Marangoni–Bénard problem, error is introduced at the upper boundary where the tangential stress condition is not satisfied by the trial functions, equations (4.7) and (4.8). Second, the boundary conditions in the previous gravity-modulated Rayleigh–Bénard studies (Gresho & Sani 1970; Gershuni *et al.* 1970; Saunders *et al.* 1992; Terrones & Chen 1993) were symmetric, leading to disturbance velocity and temperature profiles that varied in magnitude but maintained reasonably constant profile shapes. For the Marangoni instability a boundary layer profile develops that can vary considerably in both shape and magnitude for different wavenumbers. Finally, results in Gresho & Sani (1970) are presented for a value of $Pr\, g_1/\Omega^2 = 7 \times 10^{-5}$, while results in figure 14 exceed this value by two to four orders of magnitude. Nonetheless, the accuracy and qualitative agreement of the one-term approximation in figure 14(*a–d*) justify exploring the damped pendulum analogy to better understand the stability characteristics observed for the higher-order results discussed earlier.

Computing the inner products with the trial functions in equations (4.7) and (4.8), leads to relatively simple expressions for ς, ξ, and q:

$$\varsigma = \frac{1}{\Omega}\left(Pr\frac{0.02438\alpha^4 + 0.5706\alpha^2 + 6}{0.02438\alpha^2 + 0.2853} + \alpha^2 + 2.471\right), \tag{4.9}$$

$$\xi = \left(\frac{4\,Pr}{\Omega^2}\right)\frac{\alpha^6 + 25.87\alpha^4 + (303.9 - 8.035\,Ma - 0.8042\,g_0 Ra)\alpha^2 + 608.1}{\alpha^2 + 11.70}, \tag{4.10}$$

$$q = \left(\frac{-2\,g_1\,Pr\,Ra}{\Omega^2}\right)\left(\frac{0.01961\alpha^2}{0.02438\alpha^2 + 0.2853}\right). \tag{4.11}$$

As discussed in § 3.2, an α value of 2 is reasonable for the modulated problem herein. On substituting $\alpha = 2$ into the above expressions for ς, ξ, and q, equation (4.2) becomes

$$0 = \ddot{B} + \frac{2}{\Omega}(22.65\,Pr + 6.471)\dot{B} + \frac{4\,Pr}{\Omega^2}(146.6 - 2.047\,Ma - 0.2049\,g_0\,Ra - 0.2049\,g_1\,Ra\,\cos 2\tau)B. \tag{4.12}$$

https://doi.org/10.1017/S0022112001003603 Published online by Cambridge University Press

Examination of equations (4.3), (4.9), and (4.12) reveals that the Prandtl number is the only fluid transport parameter affecting damping. Furthermore, since Pr is always positive, the damping is therefore always positive. By setting the modulation amplitude, q, to zero in equation (4.2), equation (4.12) reduces to an autonomous equation, and upon rearranging yields the form of Nield's approximate result, $Ma_c/Ma_1 + Ra_c/Ra_1 = 1$, for the combined Rayleigh–Bénard/Marangoni–Bénard problem. Here, $Ma_1 = 71.62$ and $Ra_1 = 715.5$.

Damping reduces the growth rate of the undamped system as observed from the transformation required to obtain equation (4.5). The Marangoni and Rayleigh numbers are both found in the stiffness coefficient, ξ , and reinforce each other. The stabilizing (destabilizing) effect at larger modulation frequencies with increasing Pr, can be explained by the effect of the damping parameter reducing a for larger damping in equation (4.5). According to the one-term approximation, equation (4.12), by setting $g_0 Ra = 9.990 Ma$, a modulated Rayleigh–Bénard problem can be obtained that is equivalent to the modulated Marangoni–Bénard problem for the same modulation amplitude. This could occur by changing g_0 although this is physically awkward, while varying Ra would require adjusting g_1 to maintain the same amplitude value. Not enforcing these conditions demonstrates the otherwise incompatibility of the modulated Rayleigh–Bénard and Marangoni–Bénard problems noted in § 3.2.

4.3. *Method of averaging*

Although the one-term approximation is an immense simplification of the original problem posed by equations (2.6) to (2.9*c*), approximate methods are still required to investigate the Mathieu equation and its stability behaviour. The method of averaging is well suited for these purposes since the averaging process results in an autonomous set of equations. Bogoliubov & Mitropolsky (1961) provide a detailed account of the method of averaging as applied to several classical problems including the damped Mathieu equation, which is similarly presented in more recent texts (Minorsky 1962; Meirovitch 1988). Following Bogoliubov & Mitropolsky, simple stability criteria for the modulated problem can be obtained which are valid for small parameter values (damping and amplitude coefficients).

The form of equation (4.2) differs only slightly from the Mathieu problem solved by Bogoliubov & Mitropolsky, and an identical averaging procedure is applied. The resulting set of averaged equations is autonomous and to $O(\epsilon)$ leads to a concise stability criterion, $(-\xi) \leqslant q^2/2$, where $-1 < \xi < 0$. Therefore to stabilize the slightly unstable system, the square of the amplitude coefficient, q, in equation (4.2) must be at least twice the stiffness coefficient, ξ. In terms of the fluid transport parameters, this yields the following stabilization criterion for the modulated Marangoni/Rayleigh–Bénard problem:

$$\left(Ma \frac{a_{21} p_3}{b_1 b_2} + g_0 Ra \frac{a_{21} p_2}{b_1 b_2} + \frac{p_1 p_4}{b_1 b_4} \right) \leqslant \frac{Pr}{\Omega^2} \left(\frac{a_{21} p_3}{b_1 b_2} g_1 Ra \right)^2 \tag{4.13}$$

where the coefficients a_{ij} and b_i are defined in equation (4.1). This result also applies for the modulated Rayleigh–Bénard problem studied by Gresho & Sani (1970), where no-slip was required at both upper and lower surfaces of the fluid layer. The usual requirement for equation (4.13) to apply in this case is that the trial functions satisfy the boundary conditions, and the Ma term in equation (4.13) is neglected ($Ma = 0$).†

† At the very least the trial functions must not over-constrain the problem as would occur if we applied Gresho & Sani trial functions here.

https://doi.org/10.1017/S0022112001003603 Published online by Cambridge University Press

Since the system must be lightly damped with small modulation amplitude for equation (4.13) to be valid, α is set to 2, approximately α_c for the unmodulated system. After introducing the trial functions, equations (4.7) and (4.8), the stabilization criterion reduces to

$$0 \leqslant (2.047Ma + 0.2049g_0Ra - 146.6) \leqslant \frac{Pr}{2\Omega^2}(0.2046g_1Ra)^2. \tag{4.14}$$

Equation (4.14) clearly shows that modulation has a stabilizing effect on the destabilized Bénard system when the conditions of light damping and small modulation amplitude hold. These conditions are easily achievable for sufficiently large Ω. Therefore, equations (4.14) and (4.13) are well suited to determine Ω values below which modulation occurs or is no longer negligibly small. In certain applications such as reduced gravity fluid experiments this type of stabilization criterion can help to identify g-jitter magnitudes and frequencies that might adversely affect a proposed space flight experiment as well as establish g-tolerability requirements for such experiments (Skarda 1998*b*). For calculation purposes we note that the damping coefficient, ς, does not enter into the stability criterion at $O(\epsilon)$; however it does provide a relationship between Pr and Ω for fixed (and small) values of ς through equation (4.9).

Results from equation (4.14) are plotted in figure 15. Neutral stability curves corresponding to Pr values of 0.01, 1, and 10 are shown in figures 15(*a*), 15(*b*), and 15(*c*), respectively. Stability curves from the averaged one-term approximation, and the higher-order spectral method are shown in each plot. Equation (4.14) results are in good agreement with those from the one-term approximation; however both sets of results lie below the spectral results. Although an error between 10% and 12% is observed for both one-term and averaged results, they show good qualitative agreement with the spectral results. Applying a constant correction factor of 11% brings the one-term and averaged results into good quantitative agreement with the higher-order results as observed in figure 15(*d–f*). The corrected results are within 2% of the higher-order results for marginally stable Ma values less than 90 (13% larger than the unmodulated Ma value, 79.608). The averaged results are within $O(\epsilon)$ of the one-term ones, and when corrected also within $O(\epsilon)$ of the higher-order results, for Ma values 13% larger than the unmodulated neutral stability value. For the given parameter ranges, ϵ remained small, $\epsilon < 0.05$. While not exceeding one, the damping coefficient, ς exceeds ϵ by $O(10)$ at $Pr/\Omega^2 \approx 4 \times 10^{-5}$ ($Ma_{NS} \approx 90$). The error of the averaged results remains tolerable, but the accuracy rapidly deteriorates for $Pr/\Omega^2 > 4 \times 10^{-5}$. Highly truncated Galerkin models have been applied to a variety of problems (Finlayson 1972; Gershuni & Zhukhovitskii 1976), with several useful examples of the corrected Galerkin models contained in Finlayson.

As equations (4.13) and (4.14) suggest, the abscissa in figure 15(*a–c*) is rescaled to Pr/Ω^2 for figure 15(*d–f*). The averaged curves in figure 15(*d–f*) are clearly equivalent in this parameter space. The corrected averaged results and their close correspondence with the one-term and spectral results confirms that Ma_{NS} increases with modulation and the increase is proportional to Pr/Ω^2 in the limit of small modulation amplitude and damping. Careful inspection of figures 15(*d–f*) reveals that the one-term and spectral curves are very close but not identical for the three different Pr values. Although not entirely, a significant portion of the resonant frequency shift attributed to the relative strength of thermal and viscous damping can be accounted for through this rescaling. In terms of dimensional parameters, $Pr/\Omega^2 = \nu\mathfrak{D}/\Omega^{*2}$. Therefore, for small levels of modulation, the appropriate time scale is related to the geometric mean of the kinematic viscosity and thermal diffusivity as $t_c = d^2/\sqrt{\nu\mathfrak{D}}$. This is

https://doi.org/10.1017/S0022112001003603 Published online by Cambridge University Press

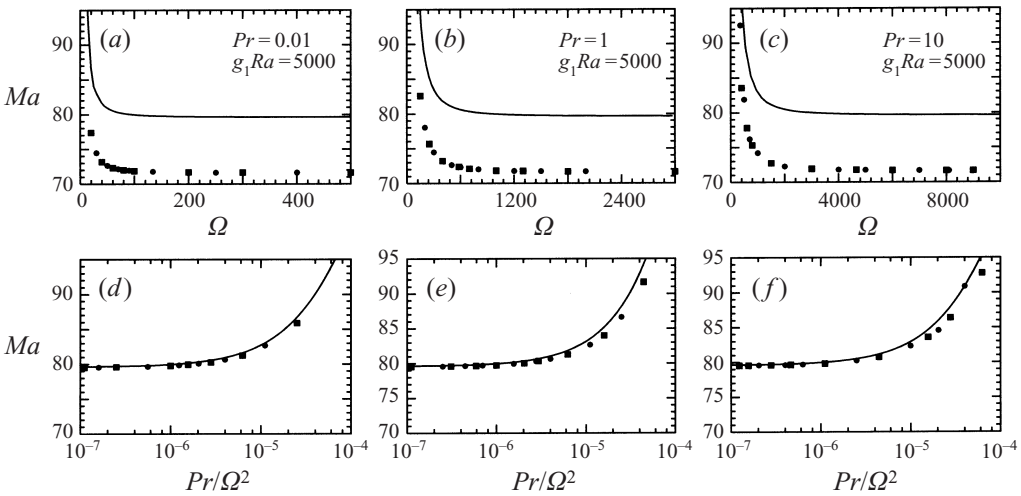


FIGURE 15. Comparison of averaged results with one-term and spectral results at marginal stable *Ma* values. Unmodulated correction factor applied to both averaged and one-term results in (*d*), (*e*) and (*f*). $\alpha = 2$. ——, higher-order spectral; ■, one-term Galerkin; ●, method of averaging.

precisely the time scale used in the studies of Gershuni and Zhukhovitskii (Gershuni & Zhukhovitskii 1963; Gershuni *et al.* 1970; Gershuni & Zhukhovitskii 1976). The thermal diffusion time scale, $d^2/\mathfrak{D}$, which was used in this study, is often applied to Bénard-type studies (Gresho & Sani 1970; Terrones & Chen 1993; Kelly & Or 1998; Or *et al.* 1999), while the viscous time scale, $t_c = d^2/\nu$, has also been used (Saunders *et al.* 1992). However, an advantage of the time scale $d^2/\sqrt{\nu\mathfrak{D}}$ is that the resonant frequency shift due to varying Pr is reduced. As the averaged results indicate, by defining a dimensionless modulation frequency, $\tilde{\Omega}$, where $\tilde{\Omega} = \Omega^* d^2/\sqrt{\nu\mathfrak{D}}$, the effects of Pr are negligible for small modulation (sufficiently large frequency).

5. Application and limitations of the analysis

To examine the usefulness and limitations of this work to physical systems it is helpful to put the results of the previous sections in the context of dimensional parameters. Here we briefly consider fluid layers of mercury and silicone oil with Pr values of 0.0125 and 105, respectively. These fluids are well characterized and have been used in previous reduced-gravity investigations. Using results of § 3.2, the Ma_c variation (with respect to the unmodulated problem), η_{Ma_c}, values are computed. For a 1 cm depth of mercury, (g_1, ω) values of (0.05, 0.03 Hz) result in an η_{Ma_c} of 10^{-4}, while (g_1, ω) values of (0.8, 0.11 Hz) lead to an η_{Ma_c} of 10^{-2}. For 1 cm depth of 10 cSt silicone oil, and (g_1, ω) of (0.6, 0.16 Hz), $\eta_{Ma_c} = 2 \times 10^{-3}$. For (0.075, 0.04 Hz), $\eta = 2 \times 10^{-5}$. At 5 cm and $g_1 \approx 10^{-2}$, η_{Ma_c} is 0.003 and 4×10^{-4}, respectively, for mercury and silicone oil; however the period is of the order of 3 minutes in both cases.

Surface deformation, which becomes important for small g_0 and d, can be characterized by the Bond number, Bo and Crispation number, Cr, where $Bo = \rho g_0 d^2/\sigma$ and $Cr = \mu\mathfrak{D}/\sigma d$. As Bo decreases and Cr increases, a long-wavelength instability eventually occurs for the unmodulated system, thus clearly placing a restriction on the flat interface results. The boundary between the long-wave and finite-wave instability can be calculated from the expression $Cr = 8.93 \times 10^{-3} Bo^{1.01}$ for the range $10^{-7} < Bo < 1$

https://doi.org/10.1017/S0022112001003603 Published online by Cambridge University Press

(Skarda & McCaughan 1999). For $Cr > 8.93 \times 10^{-3} Bo^{1.01}$ a long-wave instability occurs while a finite-wave instability occurs otherwise. Using this criterion, we can estimate g_0 levels where curvature effects are important, i.e. whether the instability is a long or finite wave mode. For unmodulated silicone oil and mercury layers, if $g_0 = 2 \times 10^{-4}$ for the 1 cm thick layer of silicone oil, Bo and Cr are 9.3×10^{-4} and 4.44×10^{-6}, respectively, which results in a finite-wave (Pearson mode) instability. Conversely if $g_0 = 10^{-4}$ ($Bo = 4.8 \times 10^{-3}$), the long-wave instability occurs. For the 1 cm deep mercury layer, $Cr = 1.5 \times 10^{-6}$, therefore, when $g_0 = 10^{-5}$ ($Bo = 3.1 \times 10^{-5}$) a finite-wave instability occurs. Using the above correlation for the long/finite-wave boundary, a finite instability is found to exist for $g_0 > 6.3 \times 10^{-6}$, and the long-wave instability occurs when the inequality is reversed.

As this investigation treats a critical limit, that of a flat (zero curvature) interface, it also raises important questions concerning the effects of curvature and the role of surface deflection. Consequently, these questions need to be answered by extending this work to include curvature effects. The resulting problem can be viewed as a combination of the Faraday instability (Benjamin & Ursell 1954) and the flat-interface modulated Bénard problem. Analogously to our examination of thermal and mechanical damping effects on the modulated Marangoni–Bénard problem, parallel investigations of the viscous Faraday instability have been presented in the literature (Kumar 1996; Cerda & Tirapegui 1998). The problem has also been studied in the broader context of a thin film flowing over a vibrated inclined plane by Woods & Lin (1995). The nature of modulated stability boundaries in the presence of long-wavelength instabilities is expected to differ from the flat-interface results. Strong evidence of this is given by the works of Or & Kelly who have examined the effects of shear modulation on both finite- and long-wavelength instabilities (Or & Kelly 1995; Or *et al.* 1999). For example, they show that the stabilizing or destabilizing effect of shear modulation depends on the preferred mode (finite or zero-wave mode) in addition to other parameters such as modulation frequency. Similarly identifying the parameter ranges where surface deflection effects are non-negligible for the modulated Marangoni–Bénard problem, will also establish the range of validity for the flat-interface approximation which was applied in this study. It would also be interesting to determine how abruptly or gradually changes occur as the finite/long-wavelength boundary is crossed. It should be noted that the zero curvature limit is typically difficult to achieve computationally, when surface deflection effects are included. Therefore the present results serve as a rigorous basis for comparison and evaluation purposes when such models approach the flat-interface limit. Alternatively, the problem can be posed from the limit of the Faraday instability, and its sensitivity to a temperature or concentration gradient examined.

6. Conclusions

Floquet theory was applied to investigate the onset of convection due to surface tension, in the presence of gravity modulation. The modulation was aligned parallel to the temperature gradient, i.e. perpendicular to the free surface. The simplest case of thermocapillary flows, the Marangoni–Bénard problem, was chosen to facilitate direct comparisons with the previously studied gravity-modulated Rayleigh–Bénard problem. This work also provides a basis for the eventual consideration of other important instability mechanisms and effects commonly associated with thermocapillary and free surface problems, e.g. surface deformation. Stability boundaries characterizing the behaviour for a wide range of fluids were computed numerically using a

https://doi.org/10.1017/S0022112001003603 Published online by Cambridge University Press

Chebyshev spectral collocation approach. A comprehensive study was performed by constructing the stability boundaries for several values of relevant parameters, such as, Pr, Ma, and g_0. One-term Galerkin and averaging methods were also used to examine an even larger range of parameter values and to develop approximate stability criteria for the modulated problem.

The stability behaviour of the Marangoni–Bénard problem is more complex in the presence of modulation. Modulation had a stabilizing effect on neutral stability curves in (α, Ma)-space at large modulation frequencies and approached the unmodulated neutral stability curve as $\Omega \to \infty$. As is typical of the modulated Rayleigh–Bénard problem, both synchronous and subharmonic regions of instability were observed for certain values of modulation frequency. For $Pr = 1$, the synchronous branch became distorted with local minima and narrow tongues forming at certain values of Ω. Sometimes both local minima were above the unmodulated Ma_c, thus resulting in a stabilizing effect. At other times one local minimum extended below the unmodulated Ma_c. Maximum stabilization occurred at some finite value of modulation frequency.

In $(1/\Omega, g_1)$-space, the gravity-modulated Marangoni–Bénard problem exhibits a fundamental instability, when Ma exceeds its corresponding unmodulated neutral stability value. This is also consistent with the Rayleigh–Bénard instability behaviour. At larger amplitudes, the resonant instability regions or tongues are attained. A fundamental difference between the stability boundaries occurs when comparing the modulated Marangoni–Bénard and Rayleigh–Bénard problems. Well-defined alternating regions of harmonic and subharmonic instability are observed in $(1/\Omega, g_1)$-space, for the modulated Rayleigh–Bénard studies. However in the case of the Marangoni–Bénard problem, the fundamental instability boundary and the synchronous tongues merged for sufficiently large Ma values. Our modulated Rayleigh–Bénard results are similar in behaviour to previous results (Gershuni & Zhukhovitskii 1963; Saunders *et al.* 1992) which apply alternative sets of boundary conditions. While there are differences in disturbance boundary conditions that were applied, even among the cited literature, the qualitative nature of the results remains unchanged and consistent for all studies. Increasing Ra or g_0 did not change the fact that discrete boundaries between the fundamental instability region, subharmonic instability regions, and synchronous instability regions always existed and were visible for all Ra or g_0 values of the stability boundaries. The sequence of stability boundaries presented in § 3 track the evolution of the subharmonic, synchronous, and fundamental instability regions for increasing values of relevant parameters. This, in turn, provides insight into rather complex changes in the stability behaviour that is not so easily quantified nor readily understood in the absence of such systematic sets of stability maps.

A one-term Galerkin approximation for the combined Marangoni/Rayleigh–Bénard problem was developed that leads to the modulated-pendulum analogy similar to that derived for the Rayleigh–Bénard problem by Gresho & Sani (1970). Although additional coefficients appear in the formulation and different trial functions must be applied, Gresho–Sani growth rate maps were constructed and directly applied to the combined Ma–Ra modulated system. Results from the one-term Galerkin approximation qualitatively reflect the behaviour of the higher-order collocation scheme. Recasting the highly truncated (one-term) formulation into the Mathieu problem provides insight through analogy with the modulated pendulum. In so doing, the effects of the seven transport parameters $(Pr, Ra, Ma, \alpha, g_0, g_1, \Omega)$ on the modulated fluid layer could be examined in terms of the three Mathieu parameters a, q, and μ. After computing the Mathieu parameters using trial functions appropriate to the

https://doi.org/10.1017/S0022112001003603 Published online by Cambridge University Press

Marangoni problem, the stability can be assessed using available Mathieu stability charts such as the Gresho–Sani stability maps (Gresho & Sani 1970).

The method of averaging was used to construct a relationship to quantify modulation effects on the fundamental instability in the large-frequency limit. The first-order result, $(2.047Ma+0.2049g_0Ra-146.6) \leqslant Pr/(2\Omega^2)(0.2046g_1Ra)^2$, provides good agreement with the higher-order calculations. After applying a constant correction factor (following Finlayson 1972) for the one-term unmodulated solution, agreement was within 2% for the range $Pr/\Omega^2 < 10^{-5}$. Therefore, to first-order approximation, modulated neutral stability results collapses to a single curve for different Pr. Also consistent with the Rayleigh–Bénard problem, the time scale originally applied by Gershuni and others (Gershuni *et al.* 1970; Gershuni & Zhukhovitskii 1976), $d^2/\sqrt{v\mathfrak{D}}$, may be better suited than either diffusive or viscous time scales when characterizing resonance behaviour over a broad range of Pr (multiple fluids).

This work was supported by NASA's Microgravity Sciences Division and Atmospheric Sciences Directorate. Computations were also performed at the Institute for Computer Applications in Science and Engineering (ICASE) during the author's appointment as a visiting researcher.

REFERENCES

Abramowitz, M. & Stegun, I (Eds.) 1974 *Handbook of Mathematical Functions, With Formulas, Graphs, and Mathematical Tables*. Dover.

Adamson, A. 1982 *Physical Chemistry of Surfaces*, 2nd Edn. John Willey.

Alexander, J. 1990 Low-gravity experiment sensitivity to residual acceleration: A review. *Microgravity Sci. Technol.* **3**, 52–68.

Benjamin, T. & Ursell, F. 1954 The stability of the plane free surface of a liquid in vertical periodic motion. *Proc. R. Soc. Lond.* A **225**, 505–515.

Bogoliubov, N. & Mitropolsky, Y. 1961 *Asymptotic Methods in the Theory of Non-linear Oscilations*. Hindustan Publishing, India.

Cerda, E. & Tirapegui, E. 1998 Faraday's instability in viscous fluid. *J Fluid Mech.* **368**, 195–228.

Davis, S. 1987 Thermocapillary instabilities. *Ann. Rev. Fluid Mech.* **19**, 403–435.

DeLombard, R. 1999 SAMS acceleration measurements on Mir from May 1997 to June 1998. *NASA TM* 2000–209282 NASA Lewis Research Center.

Finlayson, B. 1972 *The Method of Weighted Residuals and Variational Principles With Application to Fluid Mechanics, Heat, and Mass Transort*. Academic Press.

Gershuni, G., Kolesnikov, A., Legros, J. & Myznikova, B. 1997 On the vibrational convective instability of a horizontal, binary-mixture layer with Soret effect. *J. Fluid Mech.* **330**, 251–269.

Gershuni, G. & Zhukhovitskii, E. 1963 On parametric excitation of convective instability. *Prikl. Mat. Mech.* **27**, 779–783.

Gershuni, G. & Zhukhovitskii, E. 1976 *Convective Stability of Incompressible Fluids*. Keter Publishing House, Jerusalem.

Gershuni, G., Zhukhovitskii, E. & Iurkov, I. 1970 On convective stability in the presence of periodically varying parameters. *J. Appl. Math. Mech.* **34**, 442–452.

Gresho, P. & Sani, R. 1970 The effects of gravity modulation on the stability of a heated fluid layer. *J. Fluid Mech.* **40**, 783–806.

Joseph, D. 1976 *Stability of Fluid Motions I*. Springer.

Kelly, R. & Or, A. 1998 Influence of temperature modulation upon the onset of thermocapillary convection. *AIAA Paper* 98-0652.

Koschmieder, E. 1993 *Benard Cells and Taylor vorticies*. Cambridge University Press.

Kumar, K. 1996 Linear theory of Faraday instability in viscous liquids. *Proc. R. Soc. Lond.* A **452**, 1113–1126.

Legros, J., Dupont, O., Queeckers, P. & Van Vaerenbergh, S. 1990 Thermohydrodynamic

https://doi.org/10.1017/S0022112001003603 Published online by Cambridge University Press

Instabilities and Capillary Flows. In *Low-Gravity Fluid Dynamics and Transport Phenomena* (ed. J. Koster & R. Sani). Progress in Astronautics and Aeronautics. AIAA.

McLachlan, N. W. 1964 *Theory and Application of Mathieu Functions*. Dover.

McPherson, K. & Hrovat, K. 2000 Summary report of mission acceleration measurements for STS-95. *NASA TM* 2000-209677. NASA Lewis Research Center.

Meirovitch, L. 1988 *Methods of Analytical Dynamics* (Textbook Reissue). McGraw-Hill.

Minorsky, N. 1962 *Nonlinear Oscillations*. Van Nostrand Company.

Mohr, P. & Taylor, B. 2000 CODATA recommended values of the fundamental physical constants: 1998. *Rev. Mod. Phys.* **72**, 51–495.

Monti, R., Langbein, D. & Favier, J. 1987 Influence of residual accelerations on fluids physics and materials science experiments. In *Fluid Sciences and Materials Science in Space, a European Perspective* (ed. H. Walter), pp. 637–680. Springer.

Murray, B., Coriell, S. & McFadden, G. 1991 The effect of gravity modulation on solutal convection during directional solidification. *J. Cryst. Growth* **110**, 713–723.

Nelson, E. 1994 An examination of anticipated g-jitter on space station and its effects on materials processing. *NASA TM* 103775. NASA Lewis Research Center.

Newland, D. 1993 *An Introduction To Random Vibrations, Spectral & Wavelet Analysis*. Longman.

Or, A. 1997 Finite-wavelength instability in a horizontal liquid layer on an oscillating plane. *J. Fluid Mech.* **335**, 213–232.

Or, A. & Kelly, R. 1995 Onset of Marangoni convection in a layer of fluid modulated by weak nonplanar oscillatory shear. *Intl J. Heat Mass Transfer* **38**, 2269–2279.

Or, A., Kelly, R., Cortelezzin, L. & Speyer, J. 1999 Control of long-wavelength Marangoni–Bénard convection. *J. Fluid Mech.* **387**, 321–341.

Ostrach, S. 1982 Low-gravity fluid flows. *Ann. Rev. Fluid Mech.* **14**, 313–345.

Pearson, J. 1958 On convection cells induced by surface tension. *J. Fluid Mech.* **4**, 489–500.

Pimputkar, S. & Ostrach, S. 1981 Convection effects in crystal grown from the melt. *J. Cryst. Growth* **55**, 614–646.

Saunders, B., Murray, B., McFadden, G., Coriell, S. R. & Wheeler, A. 1992 The effect of gravity modulation on thermosolutal convection in an infinite layer of fluid. *Phys. Fluids* A **4**, 1176–1189.

Skarda, J. 1998*a* Convective instability of a gravity modulated fluid layer with surface tension variation. *NASA Tech. Mem. 1998-207941/AIAA Paper* 98-2599.

Skarda, J. 1998*b* NASA's microgravity fluid physics program: tolerability to residual accelerations. In *17th Intl Microgravity Measurements Group Meeting, NASA CP-208414*. NASA Lewis Research Center.

Skarda, J., Jacqmin, D. & McCaughan, F. 1998 Exact and approximate solutions to the double-diffusive Marangoni–Bénard problem with cross-diffusive terms. *J. Fluid Mech.* **366**, 109–133.

Skarda, J. & McCaughan, F. 1999 Exact solution to stationary onset of convection due to surface tension variation in a multicomponent fluid layer with interfacial deformation. *Intl J. Heat Mass Transfer* **42**, 2387–2398.

Terrones, G. & Chen, C. 1993 Convective stability of gravity-modulated doubly cross-diffusive fluid layers. *J. Fluid Mech.* **225**, 301–321.

Venezian, G. 1969 Effect of modulation on the onset of thermal convection. *J. Fluid Mech.* **35**, 243–354.

Wheeler, A., McFadden, G., Murray, B. & Coriel, S. 1991 Convectives stability in the Rayleigh–Bénard and directional solidification problems: high-frequency gravity modulation. *Phys. Fluids* A **3**, 2847–2858.

Woods, D. & Lin, S. 1995 Instability of a liquid film flow over a vibrating inclined plate. *J. Fluid Mech.* **294**, 391–407.

https://doi.org/10.1017/S0022112001003603 Published online by Cambridge University Press